NATIONAL ADVISORY COMMITTEE FOR AERONAUTICS

TECHNICAL NOTE 2971

IMPINGEMENT OF WATER DROPLETS ON WEDGES AND DIAMOND

AIRFOILS AT SUPERSONIC SPEEDS

By John S. Serafini

Lewis Flight Propulsion Laboratory
Cleveland, Ohio

NACA

Washington

July 1953

AFMC

TECHNICAL

HDT

3199/41

NATIONAL ADVISORY COMMITTEE FOR AERONAUTICS

TECHNICAL NOTE 2971

IMPINGEMENT OF WATER DROPLETS ON WEDGES AND DIAMOND

AIRFOILS AT SUPERSONIC SPEEDS

By John S. Serafini

SUMMARY

An analytical solution has been obtained for the equations of motion of water droplets impinging on a wedge in a two-dimensional supersonic flow field with a shock wave attached to the wedge. The closed-form solution yields analytical expressions for the equation of the droplet trajectory, the local rate of impingement and the impingement velocity at any point on the wedge surface, and the total rate of impingement. The analytical expressions are utilized in the determination of the impingement of water droplets on the forward surfaces of diamond airfoils in supersonic flow fields with attached shock waves.

For a wedge, the results provide information on the effect of the semi-apex angle, free-stream Mach number, pressure altitude, and droplet size. For the diamond airfoil, additional calculations provide information on the effect of airfoil thickness ratio, chord length, and angle of attack.

The results for the diamond airfoils are also correlated in terms of the total collection efficiency as a function of a modified inertia parameter. The results are presented for the following range of variables: droplet diameter from 2 to 100 microns, free-stream Mach numbers from 1.1 to 2.0, pressure altitudes from sea level to 30,000 feet, free-stream static temperatures from 420° to 460° R, semi-apex angles for the wedge from 1.14° to 7.97° and corresponding diamond airfoil thickness-to-chord ratios from 0.02 to 0.14, and chord lengths from 1 to 20 feet.

INTRODUCTION

The problem of ice prevention on aircraft flying at subsonic speeds up to flight critical Mach numbers has been a subject of considerable study and research by the NACA. The recent advent of aircraft flying at transonic and supersonic speeds has required an extension of these icing studies to higher speeds. That an icing problem exists in the transonic

and supersonic speed range is verified in reference 1, which shows by an analytical investigation with experimental confirmation that diamond or symmetrical double-wedge airfoils are subject to possible icing at flight Mach numbers as high as 1.4. A similar result is expected for other airfoil shapes that are being considered for use at transonic and supersonic flight speeds.

In conducting research on the problem of ice prevention on aircraft and missiles, regardless of the magnitude of the flight speed, it is essential that the impingement of cloud droplets on airfoils and other aerodynamic bodies be determined either through theoretical calculations or through experimentation. The impingement variables which must be determined are the total water catch, the extent of impingement, and the rate of impingement per unit area of body surface. These variables can be determined analytically from calculations of the cloud-droplet trajectories obtained for the various aerodynamic bodies. Investigators have reported the results of cloud-droplet trajectories about right-circular cylinders (refs. 2 to 5) and about airfoils (refs. 6 to 9) immersed in an incompressible fluid. An evaluation of the effect of compressibility on the droplet trajectories about cylinders and airfoils up to the critical flight Mach number is presented in reference 10.

At present there exists little information on the impingement of droplets on aerodynamic bodies in a supersonic air stream. Concentration of past effort on the problems of impingement on airfoils at subsonic flight speeds and the present lack of convenient and rapid means for obtaining the rotational flow fields about airfoils at supersonic speeds are possible explanations for the scarcity of trajectory calculations for the supersonic region. An initial contribution to the solution of the over-all problem of impingement of water droplets on aerodynamic bodies at supersonic speeds is given in reference 11, which presents an analysis of the water-interception characteristics of a wedge in a supersonic flow field.

The present report extends the analysis of reference 11 and further presents an extensive study of the impingement of water droplets on two-dimensional wedges and diamond airfoils for supersonic flight speeds that result in attached shock waves and constant velocity fields behind the shock waves. For the wedge angles and diamond airfoil thickness ratios to be considered herein, the shock-wave attachment Mach number varies from a value slightly greater than 1 to about 1.4. The method employed is based on an analytical solution of the equations of motion by means of a closed-form integration. The closed-form solution yields analytical expressions for the equation of the trajectories, the local impingement efficiencies, the velocity at any point on the trajectories, and the total rate of impingement. This solution has been made possible by using an empirical relation for the drag coefficients for spheres that gives a good approximation to the experimental drag coefficients.

2782

CS-1 back

The results of calculations for the rate, extent, and distribution of the impingement of water droplets on wedges and diamond airfoils are presented herein. The ranges of variables included for the wedge are Mach number from 1.1 to 2.0; pressure altitude of sea level, 15,000 feet, and 30,000 feet; droplet diameter from 2 to 100 microns; free-stream static temperature of 420°, 440°, and 460° R; and the tangent of the semi-apex angle from 0.02 to 0.14. The ranges of variables for the diamond or double-wedge airfoil are the same as those for the wedge, and the additional variables for the diamond airfoil range from 1 to 20 feet for the chord length and from 2 to 14 percent for the thickness.

The work presented in this report was performed at the NACA Lewis laboratory.

ANALYSIS

Statement of Problem

The solution of the problem of impingement of water droplets on a two-dimensional wedge at supersonic speeds with an attached shock wave is not as difficult as that for the impingement on various airfoils at low subsonic speeds. For the wedge at supersonic speeds with an attached shock wave, the air velocity everywhere ahead of the shock wave is constant and equal to the free-stream air velocity V_1 (fig. 1). The air velocity behind the shock wave V_2 is also everywhere constant and parallel to the wedge surface. All the droplets have the same initial velocity (that of the free-stream air velocity), and their trajectories are exactly coincident with the air streamlines upstream of the shock wave. All water droplets of a given size are subjected to identical air-velocity fields, which in turn produce identical force systems downstream of the shock wave, irrespective of the point along the shock wave where the droplets cross the wave. It follows, therefore, that, for droplets of a given size, all the trajectories in a given problem are identical with respect to the point where the droplet crosses the shock wave.

By adopting a frame of reference which moves at the constant velocity of the air V_2 downstream of the shock wave, the problem of the droplet motion is reduced to the still-air problem, defined as the determination of the motion of a droplet that, having an initial velocity, is projected into quiescent air. Hence, relative to the moving frame of reference, the initial velocity of the droplet upon crossing the shock wave is equal to the vectorial difference of the free-stream air velocity V_1 and the air velocity V_2 downstream of the shock wave. Adoption of the frame of reference moving with a constant velocity reduces the problem from the solution of two simultaneous nonlinear second-order differential equations

in the fixed coordinate system to the solution of a single nonlinear
second-order differential equation in the moving coordinate system. At
any given instant, the droplet displacement relative to the point of
intersection with the shock wave in the fixed frame of reference is
obtained by adding vectorially the droplet displacement within the moving
frame of reference to the displacement of the moving frame of reference
for the same increment of time.

This general method of attack was used in reference 11, where the
one second-order differential equation representing the droplet motion
relative to the air velocity behind the shock wave was integrated graphi-
cally. However, it is possible to obtain a completely analytical solution
by means of a closed-form integration without resorting to the use of
numerical integrations or analog computing equipment, if an empirical
relation is assumed for the drag coefficient as a function of the Reynolds
number of the droplet relative to the air. It will be shown that this
closed-form integration of the still-air problem when applied to the wedge
in supersonic flow with attached shock wave yields the equations for the
trajectories of the water droplets and the droplet velocities at any point
on the trajectories and makes available relations for the rates of total
water impingement and the local rates of water impingement along the wedge
surface. Furthermore, it is shown that these equations can also be
readily applied to the determination of the droplet impingement on a
diamond airfoil in supersonic flow with attached shock waves.

Most of the usual assumptions made in the previous investigations on
impingement at subsonic speeds are also required for this investigation.
These assumptions are: (1) The water droplets are always spherical and
do not change in size, (2) the force of gravity on the droplet may be
neglected in comparison to the drag forces, (3) the drag of the air on
the droplet is that of a viscous incompressible fluid. Here it is addi-
tionally assumed that (a) the two-dimensional supersonic flow field about
the wedge is frictionless except within the infinitesimally thin attached
shock wave, (b) no condensation shock occurs and no change in phase occurs
as the water droplets traverse the oblique shock wave, and (c) the
unbalance of the forces on the water droplet from the instant it enters
the shock wave until it emerges from the shock wave can be neglected in
the calculation of the trajectories.

Equation of Droplet Motion in Moving Reference Frame

The velocity of the droplet in the moving frame of reference is

$$U = \left| \overline{V}_d - \overline{V}_2 \right| \tag{1}$$

where $\overline{V}_d$ is the droplet velocity with respect to the fixed frame of reference, and $\overline{V}_2$ is the air velocity downstream of the attached shock wave also with respect to the fixed frame of reference (fig. 1). In the frame of reference moving with the velocity $\overline{V}_2$ (air velocity downstream of shock wave), the statement of Newton's law of motion for the water droplet becomes

$$D = - C_D \left(\frac{1}{2}\right) \rho_2 \pi a^2 U^2 = \left(\frac{4}{3}\right) \pi a^3 \rho_w \left(\frac{dU}{dt}\right) \qquad (2)$$

from which

$$\frac{dU}{dt} = - \left(\frac{3}{8}\right)\left(\frac{\rho_2}{\rho_w}\right)\left(\frac{U^2}{a}\right) C_D \qquad (3)$$

A complete list of symbols is given in appendix A.

Equation (3) is the differential form of the equation of motion of a droplet which is projected with an initial velocity into a region of quiescent air (the so-called still-air problem). The shock wave is considered to be a surface of discontinuity from which the droplets emerge with a velocity V_1. In this case the initial velocity of the droplet is

$$U_i = \left| \overline{V}_1 - \overline{V}_2 \right| \qquad (4)$$

which is the magnitude of the vector difference of the air-velocity vectors upstream and downstream of the attached shock wave. As can be shown from a consideration of the continuity equation and the equation for conservation of momentum across the oblique shock wave, the velocity vector $\overline{U}_i$ is normal to the shock wave. At any subsequent instant of time the relative droplet velocity vector $\overline{U}$ retains the same angular orientation to the shock wave and changes only in magnitude.

In reference 11 the solution of equation (3) has been obtained by numerical integration. The result obtained in this manner makes it necessary to use a graphical procedure in determining the trajectories and the local rates of impingement. However, an analytical solution of equation (2), which eliminates the graphical procedure, can be obtained if the experimental values of the drag coefficient C_D are expressed in a function involving the Reynolds number Re_r. The relation is

$$C_D = \frac{24}{Re_r} (1 + \epsilon \, Re_r{}^m) \tag{5}$$

where ϵ and m are the empirical constants. This empirical relation is a valid approximation in the range of Reynolds numbers to which cloud droplets are subjected in trajectory calculations. Substitution of the expression for C_D (eq. (5)) in equation (3) results in the expression

$$\frac{dU}{dt} = \frac{d^2x}{dt^2} = - \left(\frac{9}{2}\right) \left(\frac{\mu_2}{\rho_w}\right) \left(\frac{U}{a^2}\right) \left[1 + \epsilon \left(\frac{2\rho_2 Ua}{\mu_2}\right)^m\right] \tag{6}$$

where the local relative Reynolds number $Re_r = 2\rho_2 Ua/\mu_2$. The displacement of the water droplet in the moving frame of reference is x and is measured from the air streamline which intersects the shock wave at the point where the water droplet entered the air-flow field downstream of the shock wave. The closed-form integration of the differential equation (6) is presented in appendix B. The use of $2/3$ for the exponent m and 0.158 for the value of the empirical constant ϵ in equation (5) yields an empirical curve for the drag coefficient as a function of the local Reynolds numbers that approximates very well the variation of the experimental values of the drag coefficient in the range of Reynolds numbers from 0.5 to 500. The value of $2/3$ for the exponent m also facilitates the closed-form integration of the differential equation of motion. In figure 2 a graph of the empirical relation is presented, along with the drag coefficient data of references 4 and 12.

The results of the integration are given by the following equations:

$$x = \frac{a}{3} \epsilon^{-3/2} \left(\frac{\rho_w}{\rho_2}\right) \left[Re_{r,i}{}^{1/3} \epsilon^{1/2} + \tan^{-1} \left(Re_{r,i}{}^{-1/3} \epsilon^{-1/2}\right) - \right.$$

$$\left. \frac{1}{\sqrt{\left(Re_{r,i}{}^{-2/3} \epsilon^{-1} + 1\right) e^\tau - 1}} - \tan^{-1} \sqrt{\left(Re_{r,i}{}^{-2/3} \epsilon^{-1} + 1\right) e^\tau - 1}\right] \tag{7}$$

where

τ dimensionless time variable, $(3\mu_2/\rho_w a^2)t$

$\mathrm{Re}_{r,i}$ initial value of the local relative Reynolds number Re_r,

$2a\rho_2 U_i/\mu_2$

a droplet radius, ft

ρ_w water density, 1.9398 slugs/cu ft

ρ_2 density of air behind shock wave, slug/cu ft

ϵ empirical constant of relation of drag coefficient as function
of Reynolds number, 0.158

$$U = \frac{U_i}{\mathrm{Re}_{r,i}\ \epsilon^{3/2}} \left[\left(\mathrm{Re}_{r,i}^{-2/3}\ \epsilon^{-1} + 1\right)\ e^\tau - 1\right]^{-3/2} \qquad (8)$$

and

$$x_m = \frac{a}{3}\ \epsilon^{-3/2} \left(\frac{\rho_w}{\rho_2}\right) \left(\mathrm{Re}_{r,i}^{1/3}\ \epsilon^{1/2} - \frac{\pi}{2} + \varphi\right) \qquad (9)$$

where

$$\varphi = \tan^{-1}\left(\mathrm{Re}_{r,i}^{-1/3}\ \epsilon^{-1/2}\right); \qquad 0 \leqq \varphi \leqq \pi/2$$

The intermediate steps of integration are given in appendix B.

Equation (7) and (8) give, respectively, the displacement and the
velocity of the droplet at any instant in the moving frame of reference.
The displacement of the droplet with respect to the point where it crossed
the shock wave can be obtained by a vectorial addition of the displacement
x and the displacement of the moving reference frame in the corresponding
time interval. The droplet velocity $\overline{V}_d$ relative to the fixed frame of
reference must also be obtained by the vectorial addition of $\overline{U}$
(eq. (8)) and $\overline{V}_2$ (the air velocity downstream of the shock wave). Equa-
tion (9) gives the maximum value of x that is obtained as the time of
travel in the air-flow field downstream of the shock wave approaches
infinity. The significance of this quantity will be discussed in sub-
sequent sections.

Relations Required for Application of Closed-Form Solution

to Obtain Droplet Motion and Impingement in

Fixed Reference Frame

Impingement on wedges. - For a problem of given aerodynamic conditions, the trajectories of all the water droplets for a given size are identical when the points where the droplet trajectories intersect the shock wave are superimposed. This unique characteristic of the water-droplet trajectories about a wedge in supersonic flow with an attached oblique shock wave is the result of two constant velocity fields, one upstream and one downstream of the shock wave. Therefore, only one set of equations for a single trajectory will be necessary to calculate the impingement parameters for a specified problem, including a given droplet size. The values of the initial relative velocity U_i, the initial Reynolds number $Re_{r,i}$, and the density ratio ρ_w/ρ_2 are needed for substitution in the closed-form solution of the equations of droplet motion. These values can be obtained from information available in reference 13 and from the use of simple algebraic and trigonometric relations for given values of the free-stream Mach number M_1, the free-stream static temperature t_1, the angle of surface inclination to the free-stream direction σ, the free-stream static pressure p_1, and the droplet diameter d. These relations result in the following expressions for the initial relative velocity and initial relative Reynolds number:

$$U_i = |\overline{U}_i| = V_1 \sqrt{1 + \Omega^2 - 2\Omega \cos \sigma} = V_1 \omega \qquad (10)$$

$$Re_{r,i} = 2\sqrt{\frac{\gamma}{gR}} \left(\frac{a p_1}{\mu_2 t_1^{1/2}}\right) M_1 \omega \left(\frac{\rho_2}{\rho_1}\right) \qquad (11)$$

where

$\Omega \quad V_2/V_1$

$R \quad 53.3 \text{ ft-lb/(lb)(}^\circ\text{F)}$

$\gamma \quad 1.4$

$g \quad 32.2 \text{ ft/sec}^2$

A convenient form of the solution for the impingement on a wedge or the front half of a diamond airfoil is obtained if S is defined as the distance to the point of impingement measured from the leading edge for a water droplet that enters the flow field behind the shock wave at a distance ζ above the leading edge (fig. 1). The unique relation between S and ζ in a given problem for droplets of the same size is quite readily determined by considering the displacement of the water droplets as the vectorial sum of the displacement of the water droplet relative to the moving frame of reference and the displacement of the moving reference frame relative to a fixed frame of reference (referred to wedge). Since the moving reference frame has a velocity equal to the air velocity V_2, which is constant in magnitude and parallel to the wedge surface,

only the droplet travel in the moving reference frame contains the component of droplet travel which represents the approach of the water droplet to the wedge surface. For a water droplet starting from point A and impinging on the wedge surface at point D (fig. 1), the displacement of the moving reference frame (= $V_2 t$, where t is zero at point A) is given by the displacement vector $\overline{AB}$ equal to $\overline{CD}$, and the droplet motion in the moving frame of reference is given by the displacement vector $\overline{BD}$ equal to $\overline{AC}$. Therefore, relative to the starting point at A (fig. 1), the displacement of the water droplet to the point of impingement at D is obviously equal to $(\overline{AB} + \overline{BD})$ or to $(\overline{AC} + \overline{CD})$. From figure 1 the displacement of the water droplet at the point of impingement D, measured from the leading edge at E, is given by adding the vector $\overline{EA}$ to the displacement vector from the starting point A, and the displacement of the droplet at D referred to the leading edge is

$$S = |\overline{ED}| = |\overline{EA} + \overline{AC} + \overline{CD}| = |\overline{EC} + \overline{CD}| = |\overline{EC}| + |\overline{CD}| = \zeta + \zeta' \tag{12}$$

where ζ is defined as the magnitude of the displacement vector $\overline{EC}$ and ζ' (= $V_2 t$) is defined as the magnitude of the displacement vector $\overline{CD}$ (the displacement of the moving frame of reference). As previously noted, S is the distance from the leading edge to the point of impingement of a water droplet that initially (upstream of the shock wave) was on the streamline at a distance ζ from the leading edge, measured normal to the streamlines.

The values of ζ and ζ are obtained in terms of x, the distance of travel in the moving reference frame, from simple trigonometric identities involving the various angles shown in figure 1:

$$\zeta = x \sin \theta \tan (\nu + \sigma) \tag{13}$$

where x is given by equation (7), and ν is the angle between the relative velocity vector $\overline{U}$ and the free-stream air velocity vector $\overline{V}_1$ and is given by

$$v = \sin^{-1}\left[(\sin \sigma)\frac{\Omega}{\omega}\right] \tag{13a}$$

and

$$\xi = x \sec (v+\sigma) \tag{14}$$

Substitution of equation (14) into equation (12) for the surface distance to the point of impingement yields the following:

$$S = x \sec (v+\sigma) + V_2 \left(\frac{\rho_w a^2}{3\mu_2}\right)\tau \tag{15}$$

where τ is the dimensionless time variable used in the determination of x and is defined in the previous section.

Since x is a function of τ in equations (13) and (15), the expressions for ξ and S, respectively, are functions of τ. However, since τ cannot be eliminated from equations (13) and (15), S cannot be obtained explicitly as a function of ξ. Nevertheless, the curves of ξ, the initial displacement of the water-droplet trajectory from the leading edge normal to the free-stream direction, against S, the distance to the point of impingement of the stated water-droplet trajectory, can be obtained by substitution of the same set of values for τ in the expressions for ξ and S.

An analytical expression for the local impingement efficiency, which is designated as β, can be obtained from the above expressions for ξ and S. The local impingement efficiency β is defined by the expression

$$\beta = \lim_{\Delta S \rightarrow 0}\left(\frac{\Delta \xi}{\Delta S}\right) = \frac{d\xi}{dS} = \frac{\frac{d\xi}{d\tau}}{\frac{dS}{d\tau}} \tag{16}$$

where $\Delta\xi$ is the difference in the initial displacements of two water droplets having very nearly equal initial displacements, and ΔS is the small increment of wedge surface between the points of impingement of the two water droplets. Differentiating ξ and S with respect to τ and performing the division indicated by equation (16) yield the following expression for β:

$$\beta = \frac{1}{\frac{n_2}{n_1} + \frac{n_3}{n_1}\frac{6\epsilon^{3/2}}{a}\frac{\rho_2}{\rho_w}\left[\left(Re_{r,i}^{-2/3}\epsilon^{-1} + 1\right)e^{\tau} - 1\right]^{3/2}} \tag{17}$$

where

$$n_1 = \sin \theta \tan (\nu + \sigma) \qquad (18a)$$

$$n_2 = \sec (\nu + \sigma) \qquad (18b)$$

$$n_3 = V_2 \frac{\rho_w a^2}{3\mu_2} = V_2(t/\tau) \qquad (18c)$$

Since β and S both are functions of τ, the local impingement efficiency β at any point on the wedge surface is determined by using the same value of τ in equations (17) and (15). The value of β that exists as the point of impingement of the water droplet on the wedge surface approaches the leading edge as a limit $(S \rightarrow 0)$ is defined and given by the following:

$$\beta_0 = \lim_{S \longrightarrow 0} [\beta] = \frac{1}{\dfrac{n_2}{n_1} + \dfrac{n_3}{n_1}\left(\dfrac{3}{a^2}\dfrac{\mu_2}{\rho_w}\dfrac{1}{U_i}\right)} = \sin \sigma \qquad (19)$$

The magnitude and direction of the droplet velocity at the point of impingement $V_{d,im}$ (relative to the fixed frame of reference) can also be easily obtained at any point on the wedge surface as

$$V_{d,im} = V_1 \sqrt{\Omega^2 + \omega^2 \left(\frac{U_{im}}{U_i}\right)^2 + 2\Omega\,\omega \left(\frac{U_{im}}{U_i}\right) \cos (\nu + \sigma)} \qquad (20)$$

$$\kappa_{im} = \sigma - \sigma'_{im} = \sigma - \sin^{-1}\left[\left(\frac{U_{im}}{V_{d,im}}\right) \sin (\nu + \sigma)\right] \qquad (21)$$

where κ is the angle between the free-stream velocity vector $\overline{V}_1$ and the droplet velocity vector $\overline{V}_d$, and σ' is the angle between the droplet velocity vector $\overline{V}_d$ and the air velocity vector $\overline{V}_2$. In equations (20) and (21) for a given trajectory, V_1, Ω, ω, U_i, ν, and σ are constants. Therefore, for a given trajectory, $V_{d,im}$ and κ_{im} are functions only of U (eq. (8)) which is in turn a function of τ, the dimensionless time variable.

Impingement on diamond airfoils. - The impingement on a diamond air-
foil may be obtained from the solution to the problem of impingement on
a wedge as presented heretofore. In this report a diamond airfoil is
considered to be a symmetrical double-wedge airfoil, the maximum thickness
of which occurs at 50 percent of chord (fig. 3). At zero angle of attack,
the impingement on a diamond airfoil will be limited to the region from
the leading edge to the shoulder at 50 percent of chord. The solution
for impingement on a wedge surface having a given semi-apex angle σ (the
angle of inclination of either wedge surface to the free-stream direction)
can also be used as the solution for a diamond airfoil where the thickness
ratio of the diamond airfoil is equal to $\tan \sigma$, the tangent of the semi-
apex angle, and where the droplet size and other parameters of the problem
are the same as for the wedge. Therefore, the values of the local impinge-
ment efficiencies β and β_0 at any given point on the surface will be
identical for both the wedge and diamond airfoil under the aforementioned
similarity of conditions.

The solution for the impingement on the diamond airfoil at angle of
attack can also be obtained from the solution for impingement on a wedge
as for the case of the diamond airfoil at zero angle of attack. When
the symmetrical diamond airfoil is at angle of attack α, the angle of
inclination of its forward upper surface to the free-stream direction is
equal to $(\sigma-\alpha)$ and that of the forward lower surface of the diamond
airfoil is equal to $(\sigma+\alpha)$. Therefore, the solution to the impingement
on the upper and lower surfaces of the diamond airfoil is obtained from
the solutions for impingement on wedges having the redefined semi-apex
angles of $(\sigma-\alpha)$ and $(\sigma+\alpha)$, respectively, where the droplet size and
other parameters of the problem are kept the same. For the diamond air-
foils at angles of attack having tangents equal to or greater than the
thickness ratio, the water droplets will not impinge on the upper surface.
At angles of attack having tangents greater than the thickness ratio,
some water droplets may impinge on the lower surface beyond 50 percent of
chord. These conditions are presented in figure 3, which illustrates
schematically the three conditions. For $\alpha < \tan^{-1} (T/c)$, the impinge-
ment occurs on surfaces AC and AB; for $\alpha = \tan^{-1} (T/c)$, impingement
occurs only on surface AC; for $\alpha > \tan^{-1} (T/c)$, impingement occurs on
lower surface AC and may occur on lower surface CD. However, the
condition where $\alpha > \tan^{-1} (T/c)$ is not considered herein, since the
solution presented in this report is not valid for the determination of
trajectories of droplets impinging on the surface beyond the shoulder or
50 percent of chord of the diamond airfoil (surfaces BD or CD) where
a portion of the trajectories is within the expansion zone emanating from
the shoulder.

RESULTS AND DISCUSSION

From the equations presented in the previous section and in appendix B, the impingement of water droplets on the wedge in a supersonic flow field with an attached shock wave can be calculated over a range of free-stream conditions, wedge angles, and droplet sizes. As has been previously indicated, the impingement characteristics of the diamond airfoil (at zero angle of attack and also for small values of angle of attack) can be readily determined from the impingement on wedges for similar conditions. The results for the wedge and diamond airfoil are presented and discussed separately. A comparison of the total collection efficiency and the water impingement rate for a diamond airfoil at zero angle of attack with those for a NACA 0006-64 airfoil at zero angle of attack is presented in appendix C.

Wedge

Local impingement efficiency. - The rate of water impingement on a local area of wedge or airfoil surface is proportional to a dimensionless term β, the local impingement efficiency. The local rate of water impingement in pounds per hour per square foot is

$$W_\beta = 0.329 \ V_1 w\beta$$

where β is the fractional part of the maximum water that could impinge on a local area of the wedge or airfoil, if all the droplet trajectories were parallel to each other and the surface of impingement were projected into a plane perpendicular to the trajectories. The local impingement, when given as a function of the surface distance of the wedge, allows the determination of the local rate of impingement of water droplets at any point on the surface, the total impingement of water droplets on the entire surface or any given portion of the surface, and the extent of impingement on the surface. The local impingement efficiency β is related to a point at a given distance S on the wedge surface in equations (15), (17), and (19) by the dimensionless time variable τ, which is common to all three expressions. The variation of the local impingement efficiency β with S, the surface distance along the wedge, is presented in figure 4 for an extensive range of free-stream conditions, semi-apex angles, and droplet sizes. The values of β at the leading edge $(S \rightarrow 0)$ is the sine of the semi-apex angle $(\sin \sigma)$; and as S increases, the value of β decreases rapidly and approaches the value of zero asymptotically as S approaches infinity. However, it is to be noted that negligibly small values of β ($\beta \approx 1$ percent of β_0 for the wedge) are attained at large but finite values of S.

The curves of β as a function of S presented in figure 4 are those of an idealized situation. The assumed two-dimensional supersonic flow field about the wedge does not account for a stagnation point that must exist at the leading edge of the wedge, regardless of the sharpness of the leading edge. In addition, the leading edge of wedges and diamond airfoils might be considered to be somewhat rounded when subjected to considerable magnification. Therefore, it is reasonable to assume that very near the leading edge $(S \rightarrow 0)$ the value of β would actually be greater than the calculated value of β at the given distance S. However, this should have a negligible effect on the rest of the β curve and also on the total impingement on the wedge, since the effect of a stagnation point would be limited to a very small region about the leading edge.

For S approaching very large values, the calculated values of β probably differ somewhat from actual values obtained in flight, because the analytical solution of the present report does not consider the existence of the boundary layer on the wedge surface. Since the boundary-layer thickness increases with the surface distance along the wedge, droplets which impinge at large distances from the leading edge actually would have traveled through the boundary layer for some non-negligible interval of time. However, only a very small fraction of the total water droplets of a given size impinge under this condition, and for large values of S the values of β are negligibly small. For example, in figure 4(a) such would be the case for values of S greater than 8 or 9 feet, where $\beta < 0.0002$ as compared with $\beta_0 = 0.02$.

A preliminary survey disclosed a negligible effect of the free-stream static temperature on the local impingement efficiency as a function of the surface distance along the wedge (β against S). Values of β and corresponding values of S were calculated for free-stream static temperatures of $420°$, $440°$, and $460°$ R, for a free-stream Mach number of 1.3, pressure altitude of 15,000 feet, droplet diameter of 20 microns, and tangent of the semi-apex angle of 0.06. The values of β for the free-stream static temperature of $420°$ and $460°$ R are within 1 percent of the values of β at the free-stream static temperature of $440°$ R. Since these calculations show that curves of β against S for the three values of free-stream static temperature form practically a single curve when plotted to the usual scales, no figures are presented herein to illustrate the effect of free-stream static temperature on impingement. Furthermore, the results included herein, which are calculated for a free-stream static temperature of $440°$ R, may be used in the range of temperature from $420°$ to $460°$ R or possibly an even greater range of temperature.

The effect of the free-stream static pressure on the local impingement efficiency as a function of the surface distance along the wedge (β against S) is presented in figure 4(a) for pressure altitudes of

sea level, 15,000, and 30,000 feet. Increasing the pressure altitude
(decreasing the free-stream static pressure) increases the values of β
at any distance S. For example, at S = 1.5 at sea level, β is 0.0052;
and at 30,000 feet, β is 0.0071. Since β_0 (the value of β at
S = 0) is equal to the sin σ, where σ is the semi-apex angle, the
curves for the three pressure altitudes have the same maximum value of β.
Also,, for the various pressure altitudes the extent of impingement along
the wedge surface is essentially the same.

The effect of the semi-apex angle σ of the wedge on the local
impingement efficiency as a function of the surface distance along the
wedge is presented in figure 4(b) for values of tan σ from 0.02 to 0.10.
Since the values of β_0 are equal to sin σ, increasing the semi-apex
angle of the wedge results in an increase of β_0. The surface extent of
perceptible impingement (as characterized by $\beta \approx 0.01 \, \beta_0$) does not
vary as the wedge thickness is increased.

The effect of free-stream Mach number on the β curve is presented
in figure 4(c). The curves of β as a·function of S are given for
free-stream Mach numbers of 1.2, 1.3, 1.4, 1.5, and 2.0. For the wedge
semi-apex angle presented in the figure (tan σ = 0.04), the value of
M_1 = 1.2 is close to the shock-wave attachment Mach number. The shock-
wave attachment Mach number is a function of the wedge semi-apex angle
and is defined as that Mach number below which the shock wave is detached
from the wedge. An increase in the free-stream Mach number M_1 results
in an increased surface extent of perceptible impingement and also in an
increased value of β at any given distance S (except at S = 0, where
$\beta \equiv \beta_0 \equiv$ sin σ and at S $\rightarrow \infty$, where $\beta \rightarrow 0$). The increase in the sur-
face extent of perceptible impingement is shown in figure 4(c), in which
for free-stream Mach numbers of 1.2, 1.3, 1.4, 1.5, and ·2.0 the surface
extents of perceptible impingement on the wedge (where $\beta \approx 0.01 \, \beta_0$) are
5.35, 6.05, 6.65, 7.20, and 9.4 feet, respectively.

The effect of the droplet size on β is presented in figure 4(d)
for droplet diameters of 10, 20, 30, 40, 50, and 100 microns. The surface
extent of impingement and the values of β at any given distance S are
considerably increased as the droplet size is increased. For example,
for the semi-apex angle presented in the figure (tan σ = 0.06), at
S = 3 feet the values of β are 0.0000, 0.0033, 0.0106, 0.0182, 0.0244,
and 0.0417 for values of droplet diameter of 10, 20, 30, 40, 50, and
100 microns, respectively. The surface extent of perceptible impingement
has values of 1.5, 5.7, 11.2, 18.1, and 28.0 feet for droplet diameters
of 10, 20, 30, 40, and 50 microns, respectively. As shown by the pre-
ceding discussion and also by a comparison of the values of β as a
function of S (fig. 4)., varying the droplet diameter from 20 to
30 microns or from 30 to 40 microns is of the same order of magnitude in

its effect on the β against S curve as varying the pressure altitude from sea level to 30,000 feet or varying the free-stream Mach number from 1.2 to 1.5.

Total impingement on wedge. - The effect of the free-stream Mach number, the semi-apex angle of the wedge, the pressure altitude, and the droplet size on the total impingement on a wedge surface of infinite extent is given in figure 5. The total impingement is represented by ζ_m, which is the ζ of the droplet having its trajectory tangent to the wedge surface (theoretically the tangent trajectory touches the wedge surface at a point $S \to \infty$). This ζ_m can be obtained from the integration

$$\zeta_m = \int_0^\infty \beta \, dS$$

or more directly from equation (13) of the analytical solution, as

$$\zeta_m = x_m \sin \theta \tan (\nu + \sigma)$$

where x_m is given by equation (9) and is also defined in appendix A. The value for x_m is obtained from the expression for x (eq. (7)) by allowing $\tau \to \infty$. Since the droplet which enters the flow field downstream of the shock wave at a distance ζ equal to ζ_m (fig. 1) theoretically impinges on the wedge surface only as the surface distance S approaches infinity, only droplets which have a value of ζ equal to or less than ζ_m will impinge on the wedge surface of infinite extent. The rate of total water catch on one wedge surface in terms of ζ_m is given as

$$W_m = 0.329 \zeta_m V_1 w$$

where W_m is obtained in pounds per hour per foot of span, V_1 is the free-stream velocity in miles per hour, and w is the liquid-water content in grams per cubic meter. Therefore, ζ_m is directly proportional to the rate of total water catch on the entire wedge surface and is the rate of total water catch on one wedge surface per unit of span, free-stream velocity, and liquid-water content (in appropriate units).

The variation of ζ_m with the tangent of the wedge semi-apex angle, tan σ, is shown in figure 5(a) for free-stream Mach numbers of 1.2, 1.3, 1.4, and 2.0. As expected from the curves of β as a function of S,

the value of ζ_m increases as $\tan \sigma$ increases. However, the rate of the increase in ζ_m with respect to $\tan \sigma$ decreases with an increase in $\tan \sigma$. As can be seen from figure 5(a), increasing the free-stream Mach number increases the value of ζ_m for a constant value of $\tan \sigma$.

The variation of ζ_m with pressure altitude is presented in figure 5(b) for two Mach numbers. In the range of pressure altitudes from sea level to 30,000 feet, the increase of ζ_m with an increase in pressure altitude is approximately linear. The variation of ζ_m with the droplet diameter d in microns is presented in figure 5(c). In the range of droplet diameter from 10 to 100 microns, ζ_m as a function of d results in a curve that is very nearly a straight line when plotted on logarithmic paper. This linearity permits an accurate interpolation of ζ_m when calculations have been made for a few droplet diameters for a given value of wedge semi-apex angle, free-stream Mach number, and pressure altitude.

Droplet velocities at impingement. - The variation of $V_{d,im}/V_1$ (the ratio of the droplet impingement velocity to the free-stream velocity) with the surface distance along the wedge is presented in figure 6 for three cases. The three cases given in figure 6 are representative of the results when the droplet diameter d is 20 microns and the pressure altitude is 15,000 or 30,000 feet. The curves of $V_{d,im}/V_1$ as a function of S have characteristics similar to the curves which present β as a function of S. At $S = 0$, obviously, all the curves have $V_{d,im}/V_1$ equal to unity; and as S is increased, the value of the velocity ratio rapidly decreases and asymptotically approaches V_2/V_1, the ratio of the air velocity downstream of the shock wave to the air velocity upstream of the shock wave. The top curve in figure 6 illustrates a typical situation for which V_2/V_1 is very nearly unity ($\tan \sigma = 0.02$ and $M_1 = 2.0$). The two lower curves ($\tan \sigma = 0.06$ and 0.10 at $M_1 = 1.3$) are typical for cases where a stronger shock wave produced by a larger semi-apex angle results in decreased values of $V_{d,im}/V_1$ for large values of S.

Diamond Airfoil

As shown in the ANALYSIS, the local impingement efficiency β at any point on the forward surfaces of a diamond airfoil (surfaces AB and AC shown in fig. 3) can be obtained directly from the results for the local impingement efficiency as a function of the surface distance for wedges. The local impingement efficiency β may be obtained from figure 4 or equation (17).

In general, the results for the impingement on a diamond airfoil are presented in this report in terms of the total collection efficiency E_m as a function of the scale parameter ψ, in the attempt to conform with the existing literature on the impingement characteristics of airfoils. In the notation of the present report, the total collection efficiency E_m as stated in references 7 and 8 is defined as

$$E_m = \frac{|\zeta_u| + |\zeta_l|}{T} \tag{22}$$

where T is the maximum thickness of the diamond airfoil, and $|\zeta_u|$ and $|\zeta_l|$ are the absolute values of the initial displacements from the leading edge (in a direction normal to free-stream direction) of the droplet trajectories which impinge at the shoulder of the upper and lower surfaces, respectively, of the diamond airfoil. For the symmetrical diamond airfoil at zero angle of attack, $|\zeta_u|$ and $|\zeta_l|$ will be equal. For the symmetrical diamond airfoil at an angle of attack, the tangent of which is equal to the thickness ratio, the value of $|\zeta_u|$ is equal to zero.

The scale parameter ψ is calculated for the diamond airfoil at supersonic speeds as for other airfoils at subsonic speeds. It is defined as

$$\psi = \left(\frac{9c}{a}\right)\left(\frac{\rho_1}{\rho_w}\right) \tag{23}$$

where c is the chord length of the diamond airfoil. The results presented for impingement on diamond airfoils use essentially the same parameters as used for impingement on wedges. The parameters are: free-stream Mach number, pressure altitude, diamond airfoil thickness ratio, and droplet size. In addition, angle of attack and chord length are specified for the diamond airfoil.

Total collection efficiency at zero angle of attack. - The variation of the total collection efficiency E_m with respect to the scale parameter ψ is presented in figure 7 for the diamond airfoil at zero angle of attack. The effects of pressure altitude, airfoil thickness ratio, free-stream Mach number, and droplet size are shown.

The effect of pressure altitude on the variation of E_m with ψ for a 2-percent-thick diamond airfoil is given in figure 7(a) for zero angle of attack, free-stream Mach number of 1.4, droplet diameter of 20 microns, and free-stream static temperature of 440° R. The pressure

altitudes presented in the figure are for sea level, 15,000 feet, and 30,000 feet. The lines for constant values of chord length from 1 to 20 feet are also included in the figure. For the diamond airfoil subjected to a constant-velocity supersonic flow field, the total collection efficiency E_m increases as the pressure altitude is increased when the chord length and the other variables are held constant. Considering E_m as a function of scale parameter ψ where the droplet free-stream Reynolds number Re_1 is held constant yields results similar to those for airfoils having rounded leading edges at subsonic speeds. With Re_1 held constant, the value of E_m decreases as ψ increases in the manner indicated in figure 7(a). As previously mentioned, a comparison of the total collection efficiency and also the water impingement rate for a diamond airfoil at zero angle of attack with those for a NACA 0006-64 airfoil at zero angle of attack is presented in appendix C.

The effect of airfoil thickness ratio on the variation of E_m with ψ is presented in figure 7(b). The curves are presented for 2- to 14-percent-thick diamond airfoils (in steps of 2 percent) at zero angle of attack, free-stream Mach number of 1.4, pressure altitude of 15,000 feet, droplet diameter of 20 microns, and free-stream static temperature of 440° R. The droplet free-stream Reynolds number is maintained at a value of 453 for all the curves. The effect of increasing the airfoil thickness ratio is to decrease the total collection efficiency. The rate of decrease in the E_m with an increase in the airfoil thickness ratio becomes somewhat smaller as the airfoil thickness ratio increases.

The effect of free-stream Mach number on the variation of total collection efficiency E_m with scale parameter ψ is shown in figure 7(c). The curves presented are for free-stream Mach numbers of 1.1, 1.2, 1.3, 1.4, 1.5, and 2.0, 2-percent-thick diamond airfoil, zero angle of attack, pressure altitude of 15,000 feet, droplet diameter of 20 microns, and free-stream static temperature of 440° R. The results in the figure show that the collection efficiency increases as the free-stream Mach number increases. However, the increase in the total collection efficiency from the free-stream Mach number of 1.1 to 1.2 is considerably greater than the increase in efficiency from a free-stream Mach number of 1.2 to 1.3 and from 1.3 to 1.4, and so forth. Calculations for 4- and 6-percent-thick diamond airfoils indicate the same trend. For the 2-percent-thick diamond airfoil the lowest Mach number presented in figure 7(c) (M = 1.1) is quite close to the limiting Mach number for shock-wave attachment. Therefore, the rate of decrease of total collection efficiency with decreases in free-stream Mach number increases as the Mach number approaches the shock-wave attachment Mach number as a limit.

The effects of droplet size and chord length on the variation of total collection efficiency E_m with scale parameter ψ are shown in figures 7(d) and (e). Figure 7(d) presents curves of E_m against ψ for a 2-percent-thick diamond airfoil, zero angle of attack, pressure altitude of 15,000 feet, free-stream Mach number of 1.4, and free-stream static temperature of 440° R. The curves presented in the figure are for constant values of droplet diameter (d = 10, 20, 30, 40, and 50 microns) as well as for constant values of chord length (c = 1, 2, 4, 8, and 20 ft). Increasing the droplet size greatly increases the total collection efficiency. For example, at c = 8 feet, the values of E_m are 0.096, 0.310, 0.495, 0.625, and 0.711 at droplet diameters of 10, 20, 30, 40, and 50 microns, respectively. The rate of increase in the total collection efficiency as the droplet diameter increases is less for the larger droplet sizes. This effect can also be observed in figure 7(e), in which curves of E_m as a function of ψ are presented for a 6-percent-thick diamond airfoil, zero angle of attack, pressure altitude of 15,000 feet, free-stream Mach number of 1.3, free-stream static temperature of 440° R, and for droplet diameters of 2, 10, 20, 30, 40, 50, and 100 microns.

A comparison of figures 7(b) and (c) (same droplet size and pressure altitude) shows that the effect on the total collection efficiency E_m of an increase in the free-stream Mach number from 1.1 to 2.0 is, in general, of the same order of magnitude as a decrease from a 14- to a 2-percent-thick diamond airfoil. For example, for ψ of 1790 (c = 8 ft) in figure 7(b), the values of E_m decreased from 0.310 to 0.165 for an increase from a 2- to a 14-percent-thick diamond airfoil, respectively, a decrease of 0.145 in the value of E_m. For ψ of 1790 (c = 8 ft) in figure 7(c), the values of E_m increased from 0.230 to 0.400 for an increase in the free-stream Mach number from 1.1 to 2.0, respectively, an increase of 0.170 in the value of E_m.

Another comparison of figures 7(c) and (d) (same airfoil thickness ratio and pressure altitude) shows that the effect on the total collection efficiency E_m of an increase in the droplet diameter from 10 to 50 microns is much greater than an increase in the free-stream Mach number from 1.1 to 2.0. For example, for c = 8 feet in figure 7(d) the value of E_m increased from 0.095 to 0.710 for an increase in the droplet diameter from 10 to 50 microns, respectively, which is an increase of 0.615 in the value of E_m. As stated previously, for c = 8 feet (ψ = 1790) in figure 7(c) the increase in the value of E_m is 0.170 for a corresponding increase in the value of the free-stream Mach number from 1.1 to 2.0. For a constant value of the chord length, varying the pressure altitude has a relatively small effect on the total collection efficiency (fig. 7(a)).

Total collection efficiency as function of angle of attack of
diamond airfoil. - The previous discussion is concerned with the total
collection efficiencies for the diamond airfoil at zero angle of attack
only. The effect of angle of attack on the total collection efficiency
is presented in figure 8, in which the variation of E_m with the angle
of attack α is shown for 1- to 8-percent-thick diamond airfoils, inclu-
sive, pressure altitude of 15,000 feet, free-stream Mach number of 1.4,
droplet diameter of 20 microns, and chord lengths of 1, 2, 4, and 12 feet.
The range in the angle of attack presented in figure 8 is from α of
zero to α of $\tan^{-1}$ (T/c).

The total collection efficiency decreases slightly as the angle of
attack increases. The slope of the curve of E_m against $\tan \alpha$ is zero
at $\alpha = 0$, by virtue of the symmetry of the diamond airfoil. As the
angle of attack increases, the slope of the E_m against $\tan \alpha$ curve
becomes negative, the rate of change becoming more pronounced as the
angle of attack α increases. The effect of increasing the chord length
of the diamond airfoil is to decrease slightly the rate of decrease of
E_m with respect to the angle of attack α. A significant point that is
well-illustrated in figure 8 is that, for a constant value of chord length,
there apparently exists an envelope of the family of E_m against $\tan \alpha$
curves that have the airfoil thickness ratio T/c as the parameter. This
envelope curve presents, in terms of the angle of attack, the maximum
total collection efficiency that can be obtained for a diamond airfoil of
any thickness ratio, where the droplet size, free-stream Mach number,
pressure altitude, and chord length are considered to be constant.

For the diamond airfoil at a free-stream Mach number greater than
the shock-wave attachment Mach number, the decrease in total collection
efficiency with an increase in angle of attack is opposed to the trend
experienced by rounded-leading-edge airfoils at subsonic Mach numbers
(irrespective of the symmetry of the airfoil). For the latter type of
airfoil at subsonic speeds the increase in total collection efficiency
(as defined herein) with increasing angle of attack is accounted for by
the greatly increased impingement that occurs on the lower surfaces of
these airfoils at angle of attack. The reduction of impingement occurring
on the upper surfaces of these airfoils at angle of attack is more than
balanced by the increased impingement occurring on the lower surfaces.
On the other hand, for a given diamond airfoil at supersonic speeds with
an attached shock wave, the rate of increase with angle of attack of the
impingement on the lower surface is less in magnitude than the rate of
decrease with angle of attack of the impingement on the upper surface.
This general trend for the diamond airfoil can be explained with the help
of the figure 5(a), in which the effect of $\tan \sigma$ (tangent of the semi-
apex angle) on the total impingement rate is presented for a wedge of
infinite extent.

The forward upper surface of a diamond airfoil effectively acts as the finite portion of one surface of an infinite wedge which is decreasing its semi-apex angle (effectively the thickness of wedge) as the angle of attack of the diamond airfoil increases. The forward lower surface of a diamond airfoil effectively acts as the finite portion of one surface of an infinite wedge that is increasing its semi-apex angle as the angle of attack of the diamond airfoil increases. In figure 5(a) the increase in ζ_m, which is exactly proportional to the total impingement rate (see appendix A), becomes smaller with an increase in $\tan \sigma$ (i.e., $d^2 \zeta_m / d(\tan \sigma)^2 < 0$) for all possible values of the semi-apex angle σ. For example, in figure 5(a) for the curve of $M_1 = 1.4$, the impingement on an 8-percent-thick diamond airfoil of large chord extent and at zero angle of attack would be very nearly proportional to twice the value of ζ_m at $\tan \sigma$ of 0.08 ($2\zeta_m = 0.146$ ft). The impingement for the same airfoil under the same conditions and at an angle of attack of 2.291° ($\tan \alpha = 0.04$) would be very nearly proportional to the sum of ζ_m at $\tan \sigma$ of 0.04 and 0.12 ($\zeta_{m,u} + \zeta_{m,l} = 0.046 + 0.0905 = 0.1365$ ft).

Total collection efficiency as function of modified inertia parameter. - The total collection efficiency E_m is presented in figure 9 as a function of the modified inertia parameter K_0, as suggested in reference 14. The relation for K_0 is

$$K_0 = (\lambda/\lambda_s)K$$

where K is the inertia parameter and is defined as

$$K = (2/9) \frac{\rho_w a^2 V_1}{\mu_1 c}$$

and λ is the maximum distance of travel of a droplet projected into still air with the free-stream velocity V_1. The term λ_s is the value of the maximum distance of travel λ when Stokes' law is assumed for the drag force on the droplet. Since K is equal to λ_s/c (ref. 4), K_0 may also be written as

$$K_0 = (\lambda/\lambda_s)K = \lambda/c$$

The free-stream droplet Reynolds numbers used herein in calculating K_0 range up to 2104. The empirical drag law (eq. (5)) used in this report for the droplet motion in the moving reference frame is valid up

to the Reynolds number of approximately 500. Therefore, for the values
of K_0 presented in figure 9 (and also fig. 10), the values of (λ/λ_s)
were obtained from table I of reference 4.

The correlation of the total collection efficiency as a function of
the modified inertia parameter K_0 is shown in figure 9(a) for pressure
altitudes of sea level, 15,000, and 30,000 feet, and for droplet diameters
varying from 2 to 100 microns. For the 6-percent-thick diamond airfoil
at $M_1 = 1.3$ and zero angle of attack presented in figure 9(a), the
droplet free-stream Reynolds number Re_1 varies from 42.1 to 2104. The
values of E_m for a given thickness ratio, Mach number, and angle of
attack generally form the basis for a single curve with a small amount of
scatter existing in the higher range of value of K_0. In the lower range
of K_0, for all the values of Re_1 the plotted points have negligible
scatter. The small scatter observed is possibly due to the existence of
a very slight trend of the E_m against K_0 curves with Re_1 for the
higher values of K_0.

The effect of increasing the thickness ratio is presented in fig-
ure 9(b) for 2-, 6-, and 12-percent thick diamond airfoils. Increasing
the thickness ratio displaces the E_m against K_0 curve toward larger
values of K_0. Changing the thickness ratio of the diamond airfoil does
not alter the shape of the curve itself.

The effect of the free-stream Mach number on the variation of E_m
with K_0 is presented in figure 9(c) for the 2-percent-thick diamond
airfoil, droplet diameter of 20 microns, pressure altitude of 15,000 feet,
and for free-stream Mach numbers of 1.1, 1.2, 1.5, and 2.0. Increasing
the Mach number displaces the entire curve of E_m against K_0 towards
smaller values of K_0. As the value of M_1 increases, the rate of dis-
placement of the curve with increasing M_1 becomes smaller. The dis-
placement of the curve obtained by increasing the Mach number from 1.1
to 1.2 is more than that obtained by increasing the free-stream Mach
number from 1.2 to 1.5 and from 1.5 to 2.0.

The total collection efficiency for a diamond airfoil can also be
considered as a function of another modified inertia parameter defined as
a relative modified inertia parameter. The relative modified inertia
parameter F_0 is based on the velocity change of the air across the shock
wave rather than on the free-stream air velocity. This modified inertia
parameter and its effect on the total collection efficiency of a diamond
airfoil are presented and discussed in appendix D.

SUMMARY OF RESULTS

This report presents an analysis of the problem of impingement of water droplets on a wedge and a diamond airfoil at supersonic speeds and with attached shock waves. When a suitable empirical relation is used for the drag coefficient of a sphere, the analysis allows a closed-form integration of the equations of motion for the water droplets. The integration results in analytical expressions for the equation of the trajectories, the droplet velocity at any point on the trajectories, the local impingement efficiencies, and the total rate of impingement. The results of the calculations of the rate, extent, and distribution of the impingement of water droplets on wedges and diamond airfoils are summarized briefly as follows (the Mach number referred to is the free-stream Mach number, which is greater than the attachment Mach number for the wedge or the diamond airfoil):

1. At a given value of Mach number, droplet size, and pressure altitude, the local impingement efficiency as a function of the dimensional surface distance is the same for both the wedge and the diamond airfoil at zero angle of attack, provided the tangent of the semi-apex angle of the wedge is equal to the diamond airfoil thickness ratio.

2. For any Mach number, pressure altitude, and droplet diameter, the value of β_0 is equal to the sine of the semi-apex angle for wedge or diamond airfoil. (β_0 is the value (maximum) of local impingement efficiency as distance from leading edge to point of impingement approaches zero.)

3. The effect of the free-stream static temperature on the local impingement efficiency and total collection efficiency is negligible for temperatures from 420° to 460° R.

4. At constant values of Mach number, droplet size, and semi-apex angle of the wedge or corresponding thickness ratio of the diamond airfoil, an increase in the pressure altitude increases slightly the local impingement efficiencies and total collection rates on wedges and diamond airfoils; but an increase in the pressure altitude has a negligible effect on the surface extent of perceptible impingement.

5. At constant values of Mach number, droplet size, and pressure altitude, increasing the thickness ratio of the diamond airfoil or corresponding semi-apex angle of the wedge increases the local impingement efficiency, has a negligible effect on the surface extent of perceptible impingement, and decreases the total collection efficiency of the diamond airfoil.

6. At constant values of droplet size, pressure altitude, and semi-apex angle of the wedge or thickness ratio of the diamond airfoil, an increase in Mach number increases both the surface extent of impingement and the value of the local impingement efficiency.

2782

7. At constant values of pressure altitude, semi-apex angle of the wedge or thickness ratio of the diamond airfoil, and Mach number, an increase in the droplet size increases considerably the surface extent of perceptible impingement, the local impingement efficiency, and total impingement rate.

8. The variation of total collection efficiency of the diamond airfoil at zero angle of attack as a function of the scale parameter for constant values of the droplet free-stream Reynolds number is similar in form to that for subsonic airfoils.

9. The total collection efficiency of the diamond airfoil decreases slightly as the angle of attack increases.

10. For a diamond airfoil of a given thickness ratio and Mach number, the values of total collection efficiency for a wide range of values of droplet free-stream Reynolds number comprise a single curve when plotted against the modified inertia parameter. The effect of increasing the thickness ratio or decreasing the Mach number is to displace the entire collection efficiency against modified inertia parameter curve in the direction of larger values of modified inertia parameter.

Lewis Flight Propulsion Laboratory
    National Advisory Committee for Aeronautics
        Cleveland, Ohio, April 21, 1953

APPENDIX A

SYMBOLS

The following symbols are used in this report:

a droplet radius, ft

c airfoil chord length, ft

C_D drag coefficient, dimensionless

D drag force on spherical water droplet, lb

d droplet diameter, microns

E_m total collection efficiency (defined by eq. (22)), dimensionless

F relative inertia parameter, $(2/9)\dfrac{\rho_w a^2 U_i}{\mu_1 c} = \dfrac{x_{m,s}}{c}$, dimensionless

F_0 relative modified inertia parameter, $\left(\dfrac{x_m}{x_{m,s}}\right)\left(\dfrac{x_{m,s}}{c}\right) = \dfrac{x_m}{c}$

g acceleration due to gravity, 32.2 ft/sec^2

K inertia parameter, $(2/9)\dfrac{\rho_w a^2 V_1}{\mu_1 c} = \dfrac{\lambda_s}{c}$, dimensionless

K_0 modified inertia parameter, $(\lambda/\lambda_s)K = \dfrac{\lambda}{c}$, dimensionless

M_1 free-stream Mach number

m empirical constant (used in eq. (5)), 2/3

n_1, n_2, n_3 constants of flow field (defined by eqs. (18a), (18b), and (18c), respectively)

p_1 free-stream static pressure, lb/sq ft

R gas constant, 53.3 ft-lb/(lb)($^\circ$F)

Re_r droplet Reynolds number relative to air behind shock wave, $2a\rho_2 U/\mu_2$, dimensionless

2782

Re_1	free-stream droplet Reynolds number, $2a\rho_1 V_1/\mu_1$, dimensionless

S distance to point of impingement measured from leading edge for a water droplet which enters the flow field behind the shock wave at a distance ζ above the leading edge (eq. (15) and fig. 1), ft

T maximum thickness of airfoil, ft

T/c ratio of maximum thickness to chord length of airfoil, dimensionless

t time, sec

t_1 free-stream static temperature, $^\circ R$

U magnitude of droplet velocity relative to air velocity downstream of shock wave, $|\overline{V}_d - \overline{V}_2|$, fps

V_d droplet velocity, fps

V_1 free-stream velocity, fps or mph

V_2 air velocity downstream of shock wave, fps

W rate of water catch, lb/(hr)(ft span)

W_β local rate of water catch, lb/(hr)(sq ft surface)

w liquid-water content of air, g/cu m

x $\int_0^t U \, dt$, displacement of droplet in moving frame of reference (relative to air stream), where $t = 0$ the instant the water droplet intercepts the shock wave

x_m maximum value of displacement x as $\tau \to \infty$ as a limit (maximum distance of travel of droplet projected into still air with relative velocity U_i), ft

$x_{m,s}$ value of maximum distance of travel x_m obtained by assuming Stokes' law for drag force on droplet, ft

α angle of attack of airfoil, deg

β local impingement efficiency, $d\zeta/dS$, dimensionless

β_0 maximum value of β as $S \rightarrow 0$; $\beta_0 \equiv \sin \sigma$, dimensionless

γ ratio of specific heats (1.4 for air)

ϵ empirical constant (used in eq. (5)), 0.158, dimensionless

ζ initial displacement of droplet trajectories from leading
            edge in direction normal to free-stream direction (eq. (13))

ζ_m maximum value of initial displacement ζ for a droplet
            obtained when its trajectory is tangent to wedge surface
            (theoretically as $S \rightarrow \infty$)

ζ_u, ζ_l absolute values of initial displacement from leading edge
            (in direction normal to free-stream direction) of droplet
            trajectories which impinge at shoulder of upper and lower
            surfaces, respectively, of diamond airfoil

η distance along shock wave measured from wedge apex to point
            where droplet trajectory intercepts shock wave

θ shock-wave angle

κ angle between free-stream velocity vector $\overline{V}_1$ and droplet
            velocity vector $\overline{V}_d$

λ maximum distance of travel of droplet projected into still air
            with free-stream velocity V_1, ft

λ_s value of distance of travel λ obtained by assuming Stokes'
            law for drag force on water droplet, ft

μ_1 dynamic viscosity at free-stream static temperature,
            (lb)(sec)/sq ft

μ_2 dynamic viscosity at static temperature downstream of shock
            wave, (lb)(sec)/sq ft

ν angle between free-stream velocity vector $\overline{V}_1$ and initial
            relative velocity vector $\overline{U}_i$, (defined by eq. (13a))

ξ, ξ' components of droplet displacement referred to wedge surface
            (defined by eq. (12)), ft

ρ_w water-droplet mass density, 1.9398 slugs/cu ft

ρ_1 free-stream mass density of air, slug/cu ft

ρ_2 mass density of air downstream of shock wave, slug/cu ft

σ semi-apex angle

σ' angle between droplet velocity vector $\overline{V}_d$ and velocity

        vector $\overline{V}_2$

τ dimensionless time variable, $(3\mu_2/\rho_w a^2)t$

φ phase angle, $\tan^{-1}(Re_{r,i}^{-1/3}\epsilon^{-1/2})$, $0 \leqq \varphi \leqq \pi/2$ (eq. (9))

ψ scale parameter, $(9c/a)(\rho_1/\rho_w)$

Ω ratio of air velocity downstream of shock wave to free-stream

        velocity V_2/V_1

ω ratio of initial droplet relative velocity to free-stream

        velocity U_i/V_1

Subscripts:

i   initial (at shock wave)

im   impingement

l lower

m   maximum

u   upper

Barred symbols denote vectorial quantities.

APPENDIX B

CLOSED-FORM INTEGRATION OF EQUATION OF MOTION

(RELATIVE TO AIR FLOW DOWNSTREAM OF SHOCK WAVE)

This appendix provides the various steps necessary to the closed-form integration of equation (6), which is the differential equation of motion of the water droplet in the moving reference frame. The differential equation of motion (6) can be rewritten as

$$\frac{dU}{dt} = - \left(\frac{A_2}{A_1}\right)\left(\frac{24U}{a^2}\right)(1 + \epsilon A_1{}^m U^m a^m) \tag{B1}$$

where for convenience

$$Re_r = A_1 U a \tag{B2}$$

$$A_1 = \frac{2\rho_2}{\mu_2} \tag{B3}$$

$$A_2 = \frac{3}{8}\frac{\rho_2}{\rho_w} \tag{B4}$$

(A complete list of symbols is given in appendix A.) Algebraic simplification and rewriting result in the form

$$dt = - \frac{A_3\ dU}{U(1 + A_4 U^m)} \tag{B5}$$

where

$$A_3 = (A_1/A_2)(a^2/24) \tag{B6}$$

and

$$A_4 = \epsilon A_1{}^m a^m \tag{B7}$$

2782

Equation (B5) is not readily integrable in its present form. By letting

$$p = U^m \qquad (B8)$$

and

$$p' = p/p_i = U^m/U_i{}^m \qquad (B9)$$

equation (B5) becomes

$$dt = - (A_3/m)(dp'/p') + (A_3/m) \frac{A_4 p_i \; dp'}{(1 + A_4 p_i p')} \qquad (B10)$$

This form of the equation is readily integrated, and upon resubstituting the relations (B8) and (B9), there is obtained the following expression for the velocity of the droplet as a function of the time t:

$$U = U_i \left\{ \exp\left[(t-B_1)\frac{m}{A_3}\right] - U_i{}^m A_4 \right\}^{-1/m} \qquad (B11)$$

where B_1 is the constant of the integration.

Since $U \equiv \frac{dx}{dt}$, equation (B11) can be rewritten in integral form as

$$\int dx = \int U_i \left\{ \exp\left[(t-B_1)\frac{m}{A_3}\right] - U_i{}^m A_4 \right\}^{-1/m} dt + B_2 \qquad (B12)$$

where B_2 is the second integration constant. Equation (B12) requires simplification before a closed-form integration can be performed. Consider the following substitutions:

$$y = \left(\frac{m}{A_3}\right) t \qquad (B13)$$

$$A_5 = \frac{A_3}{m} U_i \left(U_i{}^m A_4\right)^{-1/m} = \frac{A_3}{m} \left(A_4\right)^{-1/m} \qquad (B14)$$

$$A_6 = \left(U_i{}^m A_4\right)^{-1} \exp(-B_1 m/A_3) \qquad (B15)$$

By using the substitutions given by (B13), (B14), and (B15), it is possible to write equation (B12) as

$$\int dx = \int A_5 \left(A_6 e^y - 1\right)^{-1/m} dy + B_2 \qquad (B16)$$

Before further steps can be taken in the closed-form integration of the equation of motion of the droplet, it is necessary to determine the value of the empirical constant m. It is noted that in approximating the curve of the drag coefficient as a function of the local Reynolds number by a relation of the form given by

$$C_D = (24/Re_r)(1 + \epsilon Re_r^m) \qquad (5)$$

it is possible to consider that the value of m is 2/3 and the value of ϵ is 0.158. That the approximation of the experimental curve by the empirical relation is very good in the range of Reynolds numbers from about 0.5 to 500 can be seen by referring to figure 2, which presents a graph of the empirical relation along with the drag-coefficient data of references 4 and 12.

The use of $m = 2/3$ in equation (B16) along with the substitution

$$e^y = q \qquad (B17)$$

and the use of formulas of integration given on pages 16 and 17 of reference 15 allow equation (B16) to be integrated as shown in the following steps:

$$\int dx = \int \frac{A_5\, dq}{q(A_6 q - 1)^{3/2}} + B_2$$

$$\int dx = -\int \frac{A_5\, dq}{q(A_6 q - 1)^{1/2}} + A_6 \int \frac{A_5\, dq}{(A_6 q - 1)^{3/2}} + B_2$$

$$\frac{x - B_2}{2A_5} = -\frac{1}{\sqrt{A_6 q - 1}} - \tan^{-1}\sqrt{A_6 q - 1} \qquad (B18)$$

If the original time or independent variable t is reintroduced into equation (B18) and the substitutions are made for A_5 and A_6, the equation has the form

$$\frac{(A_4)^{3/2} (B_2-x)}{3A_3} = \frac{(A_4 U_i^{2/3})^{1/2}}{\sqrt{\exp\left[\frac{2(t-B_1)}{3A_3}\right] - A_4 U_i^{2/3}}} +$$

$$\tan^{-1}\left[\frac{1}{(U_i^{2/3} A_4)^{1/2}} \sqrt{\exp\left[\frac{2(t-B_1)}{3A_3}\right] - A_4 U_i^{2/3}}\right] \qquad \text{(B19)}$$

Substituting for A_3 and A_4 (except in the exponent of e) in equation (B19) results in

$$\frac{(B_2-x)}{a}\left[3\epsilon^{3/2}\left(\frac{\rho_2}{\rho_w}\right)\right] = \frac{\text{Re}_{r,i}^{1/3} \epsilon^{1/2}}{\sqrt{\exp\left[\frac{2(t-B_1)}{3A_3}\right] - \text{Re}_{r,i}^{2/3} \epsilon}} +$$

$$\tan^{-1}\left[\frac{1}{\text{Re}_{r,i}^{1/3} \epsilon^{1/2}} \sqrt{\exp\left[\frac{2(t-B_1)}{3A_3}\right] - \text{Re}_{r,i}^{2/3} \epsilon}\right] \qquad \text{(B20)}$$

Equation (B20) is the integrated equation with undetermined integration constants for the motion of the water droplets relative to the air velocity behind the shock wave. The integration constants are determined from the boundary conditions, which are

$$U = U_i$$

$$\text{at} \quad t = 0$$

$$x = 0$$

The substitution of the boundary conditions, and thus the determination of the integration constants B_1 and B_2, results in the final form of the integrated equation of motion for the water droplets relative to the air velocity downstream of the shock wave as follows (in the frame of reference moving with the constant velocity V_2):

$$x = \frac{a}{3} \epsilon^{-3/2} \left(\frac{\rho_w}{\rho_2}\right) \left[\mathrm{Re}_{r,i}^{1/3} \epsilon^{1/2} + \tan^{-1}\left(\mathrm{Re}_{r,i}^{-1/3} \epsilon^{-1/2}\right) - \right.$$

$$\left. \frac{1}{\sqrt{\left(\mathrm{Re}_{r,i}^{-2/3} \epsilon^{-1} + 1\right) e^{\tau} - 1}} - \tan^{-1} \sqrt{\left(\mathrm{Re}_{r,i}^{-2/3} \epsilon^{-1} + 1\right) e^{\tau} - 1} \right]$$

<div align="right">(7)</div>

where

τ dimensionless time variable, $(3\mu_2/\rho_w a^2)t$

$\mathrm{Re}_{r,i}$ initial value of local relative Reynolds number, Re_r, $2a\rho_2 U_i/\mu_2$

a droplet radius, ft

ρ_w water density, 1.9398 slugs/cu ft

ρ_2 density of air behind shock wave, slug/cu ft

ϵ empirical constant of relation of drag coefficient as function of Reynolds number, 0.158

The final form of the corresponding equation for the relative velocity of the water droplet as a function of the dimensionless time variable τ is obtained from equation (B11) as

$$U = \frac{U_i}{\mathrm{Re}_{r,i} \epsilon^{3/2}} \left[\left(\mathrm{Re}_{r,i}^{-2/3} \epsilon^{-1} + 1\right) e^{\tau} - 1 \right]^{-3/2} \tag{8}$$

It can be seen from equations (7) and (8) that as t approaches infinity the value of U approaches zero and that a limit exists for the value of x as t approaches infinity. This limiting value of x is

$$x_m \approx \frac{a}{3} \epsilon^{-3/2} \left(\frac{\rho_w}{\rho_2}\right) \left(\mathrm{Re}_{r,i}^{1/3} \epsilon^{1/2} - \frac{\pi}{2} + \varphi\right) \tag{9}$$

where

$$\varphi = \tan^{-1}\left(\mathrm{Re}_{r,i}^{-1/3} \epsilon^{-1/2}\right); \quad 0 \leqq \varphi \leqq \frac{\pi}{2}$$

APPENDIX C

COMPARISON OF COLLECTION EFFICIENCY AND IMPINGEMENT RATE FOR

DIAMOND AIRFOIL WITH THOSE FOR NACA 0006-64 AIRFOIL

A comparison of the total collection efficiency as a function of a
modified inertia parameter K_0 for a diamond airfoil at supersonic
speeds (attached shock wave) with that for the NACA 0006-64 airfoil
(ref. 9) at free-stream Mach numbers less than critical is presented in
figure 10. Both airfoils are 6-percent thick and are at zero angle of
attack. It is important to keep in mind that figure 10 does not allow
a comparison of the two airfoils at the same Mach number, and such a
comparison cannot be made, because the analysis for the NACA 0006-64
airfoil is not valid above the critical Mach number and that for the
diamond airfoil is not valid below the shock-wave attachment Mach number.
It is, however, of value to consider a comparison of the two airfoils
with each operating within its appropriate speed range. In figure 10
the rate of increase in E_m with respect to K_0 is greater for the
diamond airfoil than for the NACA 0006-64. For a constant droplet size,
pressure altitude and temperature, and free-stream Mach number resulting
in a constant value of λ, K_0 varies inversely as the chord length
$(K_0 = \lambda/c)$. In general, therefore, the rate of decrease in E_m with
increasing chord length is greater in magnitude for the diamond airfoil
than for the NACA 0006-64 airfoil.

A comparison of the rate of total water catch per unit span for the
diamond airfoil with that for the NACA 0006-64 airfoil can be obtained
if values (necessarily different) for the free-stream Mach numbers for
the two airfoils are assigned. Assume that both airfoils are of the same
thickness ratio and chord length. Further, assume that the diamond air-
foil and NACA 0006-64 airfoil encounter identical icing conditions of
droplet diameter (20 microns), pressure altitude and temperature
(15,000 ft and 440° R), and liquid-water content (0.5 g/cu m), but have
free-stream Mach numbers of 1.5 and 0.75, respectively. For the static
temperature assumed, the Mach numbers of 1.5 and 0.75 correspond to speeds
of 1051 miles per hour and 526 miles per hour, respectively. Therefore,
the magnitudes of the inertia parameter K and the free-stream droplet
Reynolds number Re_1, for the diamond airfoil are twice as great as for the
NACA 0006-64 airfoil. Varying the chord length from 1 to 20 feet produces
a change in the value of K_0 from 0.386 to 0.0193 for the diamond air-
foil and from 0.266 to 0.0130 for the NACA 0006-64 airfoil. This vari-
ation in K_0 for both airfoils results in values of E_m which are of
the same order of magnitude. For the given icing conditions, the follow-
ing table lists for chord lengths of 4 and 20 feet the various pertinent

parameters and variables, including the rate of total water catch on the airfoil per unit span for both the 6-percent-thick diamond airfoil and the NACA 0006-64 airfoil:

6-Percent-thick diamond airfoil at $M_1 = 1.5$ $(V_1 = 1051$ mph$)$						
Chord length, c, ft	Free-stream droplet Reynolds number, Re_1*	Inertia parameter, K	$\dfrac{\lambda}{\lambda_s}$	Modified inertia parameter, K_0	Total collection efficiency, E_m	Rate of water catch, W, lb/(hr) (unit span)
4	485	0.542	0.178	0.0965	0.432	17.9
20	485	.108	.178	.0193	.111	23.0
NACA 0006-64 at $M_1 = 0.75$ $(V_1 = 526$ mph$)$						
4	243	0.271	0.246	0.0665	0.330	6.85
20	243	.0542	.246	.0130	.128	13.3

*Values of viscosity of air obtained from linear variation with temperature given in reference 16.

The rate of total water catch on the airfoil per unit span is calculated from

$$W_m = 0.329 E_m T V_1 w$$

where T is the maximum thickness of the airfoil in feet, w is the liquid-water content in grams per cubic meter, and V_1 is the free-stream velocity in miles per hour. For this particular example, the table shows that for the 4-foot chord, the diamond airfoil has a somewhat larger value of E_m than the NACA 0006-64 airfoil; and for the 20-foot chord, the opposite is the case. Comparison of the two airfoils for a given chord length shows that, as expected, the effect of the total collection efficiency on the rate of water catch is small when compared with the free-stream velocity ratio chosen (2:1). The most significant comparison to be obtained from the table is that, for the diamond airfoil, increasing the chord length by a factor of 5 (from 4 to 20 ft) results in an increase of only 28 percent in the rate of water catch; whereas, for the NACA airfoil, a like change in the chord length results in an increase of 94 percent. This difference is the result of the fact that, unlike the local impingement on the rounded leading-edge airfoils at free-stream Mach numbers less than critical, the local impingement at a given point on the surface of diamond airfoils does not vary with the chord length of the diamond airfoil, which is at a supersonic Mach number above the shock-wave attachment Mach number.

APPENDIX D

TOTAL COLLECTION EFFICIENCY OF DIAMOND AIRFOILS AS FUNCTION

OF RELATIVE MODIFIED INERTIA PARAMETER F_0

For air-flow fields that contain a shock wave, such as those con-
sidered herein, the water droplets upon crossing the shock wave suddenly
have a velocity relative to the air. For the diamond airfoil with an
attached shock wave, this initial relative velocity is the same for all
the droplets entering the air-flow field downstream of the shock wave.
As discussed in previous sections, this common initial velocity U_i may
be considered to be the initial velocity of projection of a droplet in
a reference frame having no air motion in it and moving relative to the
fixed frame of reference at the constant velocity of the air downstream
of the shock wave. Therefore, it is of interest to define a new set of
inertia parameters, F and F_0, based on the motion of the droplet in
this moving reference frame. In the expressions for Re_1, K, and K_0,
if the initial relative droplet air velocity U_i is substituted for V_1,
then

$$Re_{r,i} = \frac{\rho_1 U_i 2a}{\mu_1}$$

$$F = K \ (U_i/V_1) = (2/9) \ \frac{\rho_w a^2 U_i}{\mu_1 c} = \frac{x_{m,s}}{c}$$

and

$$F_0 = \left(\frac{x_m}{x_{m,s}}\right) F = \frac{x_m}{c}$$

where x_m (eq. (9)) is the maximum distance of travel of a droplet which
is projected into still air with the relative velocity U_i, and $x_{m,s}$
is that value of the maximum distance of travel when Stokes' law is
assumed for the drag force on the droplet.

The total collection efficiency E_m is presented in figure 11 as a
function of the relative modified inertia parameter F_0. The curves of
E_m against F_0 have exactly the same form as the curves of E_m against
K_0, except that the use of F_0 results in a displacement of the entire

curve towards smaller numerical values of the abscissa. The effect of diamond airfoil thickness ratio and of free-stream Mach number on E_m as a function of the relative modified inertia parameter F_0 is presented in figures 11(a) and (b), respectively. The displacement of the E_m against F_0 curves obtained by varying the thickness ratio (fig. 11(a)) or by varying the free-stream Mach number (fig. 11(b)) is greater than the displacement of the E_m against K_0 curves obtained by the same procedures (figs. 9(b) and (c)).

2782

REFERENCES

1. Callaghan, Edmund E., and Serafini, John S.: Analytical Investigation of Icing Limit for Diamond Airfoil in Transonic and Supersonic Flow. NACA TN 2861, 1953.

2. Glauert, Muriel: A Method of Constructing the Paths of Raindrops of Different Diameters Moving in the Neighborhood of (1) a Circular Cylinder, (2) an Aerofoil, Placed in a Uniform Stream of Air; and a Determination of the Rate of Deposit of the Drops on the Surface and the Percentage of Drops Caught. R. & M. No. 2025, British A.R.C., 1940.

3. Kantrowitz, Arthur: Aerodynamic Heating and the Deflection of Drops by an Obstacle in an Air Stream in Relation to Aircraft Icing. NACA TN 779, 1940.

4. Langmuir, Irving, and Blodgett, Katherine B.: A Mathematical Investigation of Water Droplet Trajectories. Tech. Rep. No. 5418, Air Materiel Command, AAF, Feb. 19, 1946. (Contract No. W-33-038-ac-9151 with General Electric Co.)

5. Brun, Rinaldo J., and Mergler, Harry W.: Impingement of Water Droplets on a Cylinder in an Incompressible Flow Field and Evaluation of Rotating Multicylinder Method for Measurement of Droplet-Size Distribution, Volume-Median Droplet Size, and Liquid-Water Content in Clouds. NACA TN 2904, 1953.

6. Bergrun, Norman R.: A Method for Numerically Calculating the Area and Distribution of Water Impingement on the Leading Edge of an Airfoil in a Cloud. NACA TN 1397, 1947.

7. Guibert, A. G., Janssen, E., and Robbins, W. M.: Determination of Rate, Area, and Distribution of Impingement of Waterdrops on Various Airfoils from Trajectories Obtained on the Differential Analyzer. NACA RM 9A05, 1949.

8. Brun, Rinaldo J., Serafini, John S., and Moshos, George J.: Impingement of Water Droplets on an NACA 65_1-212 Airfoil at an Angle of Attack of $4°$. NACA RM E52B12, 1952.

9. Lenherr, F. E., and Thomson, J. E.: Preliminary Report on the Computation of Water Drop Trajectories about a 6 Percent Airfoil. TDM-67, Northrop Aircraft, Inc., Aug. 14, 1952.

10. Brun, Rinaldo J., Serafini, John S., and Gallagher, Helen M.: Impingement of Cloud Droplets on Aerodynamic Bodies as Affected by Compressibility of Air Flow Around the Body. NACA TN 2903, 1953.

11. Tribus, Myron, and Guibert, Armand: Impingement of Spherical Water Droplets on a Wedge at Supersonic Speeds in Air. Jour. Aero. Sci., vol. 19, no. 6, June 1952, pp. 391-394.

12. Williams, Glenn Carber: Heat Transfer, Mass Transfer and Friction for Spheres. Sc. D. Thesis, M.I.T., 1942.

13. The Staff of the Ames 1- by 3-Foot Supersonic Wind-Tunnel Section: Notes and Tables for Use in the Analysis of Supersonic Flow. NACA TN 1428, 1947.

14. Sherman, P., Klein, J. S., and Tribus, M.: Determination of Drop Trajectories by Means of an Extension of Stokes' Law. Eng. Res. Inst., Air Res. and Dev. Command, USAF, Univ. Mich., Apr. 1952. (Contract AF 18(600)-51, Proj. M992-D.)

15. Peirce, B. O.: A Short Table of Integrals. Third ed., Ginn and Co., 1929.

16. Diehl, Walter Stuart: Engineering Aerodynamics. Second ed., The Ronald Press Co., 1936.
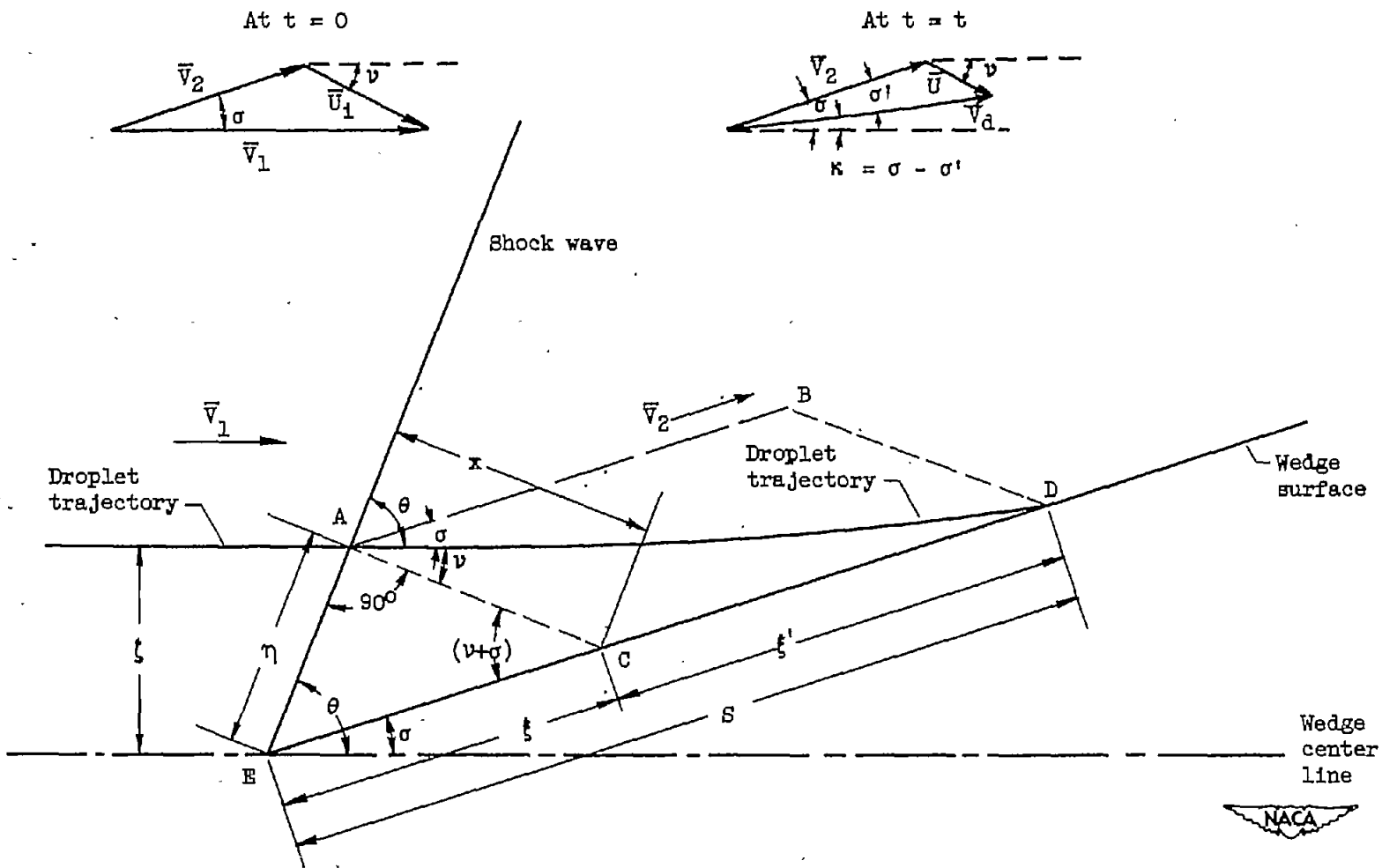
Figure 1. - Schematic diagram of water-droplet trajectory for wedge in supersonic flow with attached shock wave.
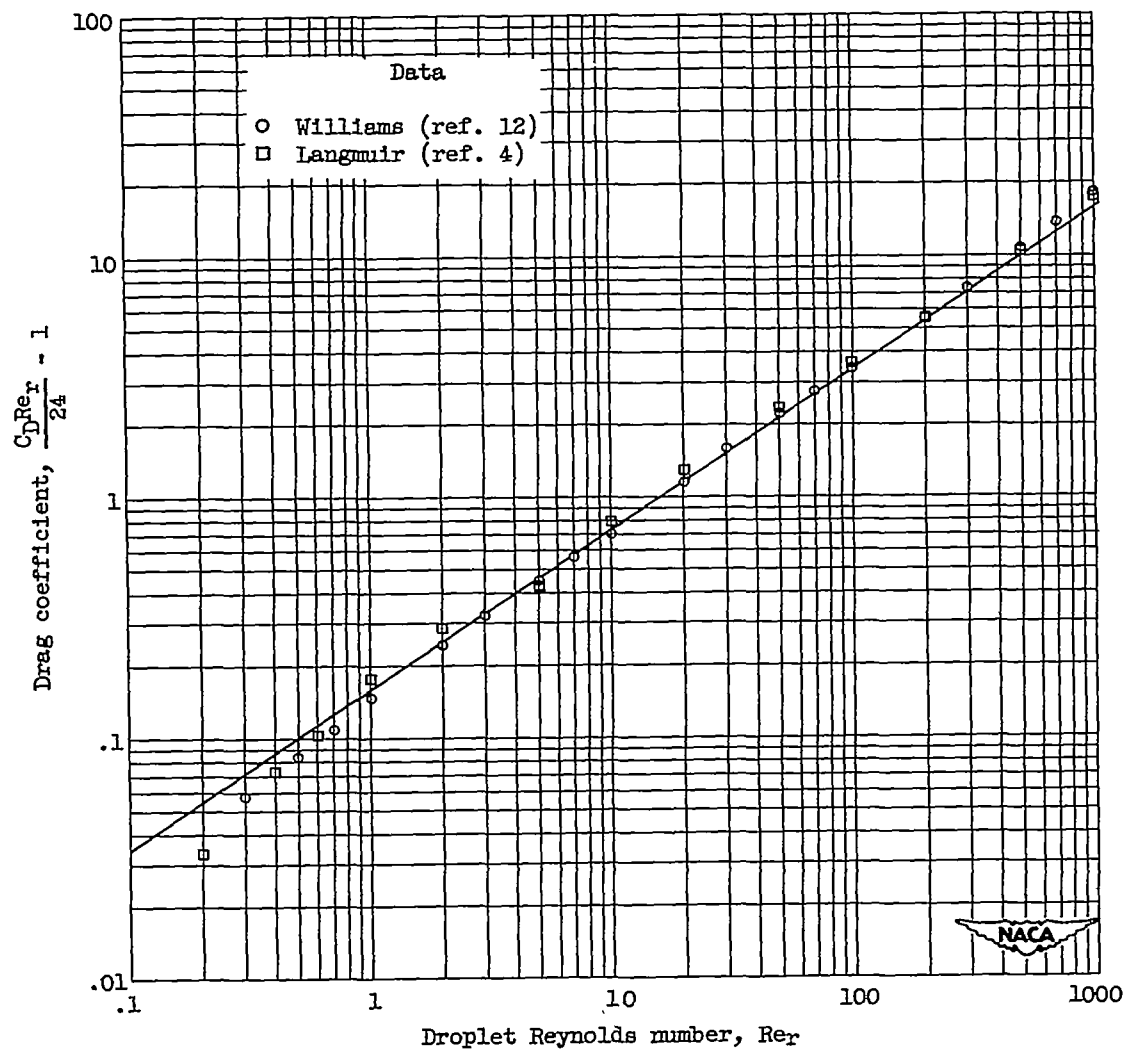
Figure 2. - Comparison of empirical relation for drag coefficient as function of droplet Reynolds number with experimental values.

$$\frac{C_D Re_r}{24} = 1 + 0.158(Re_r)^{2/3}.$$
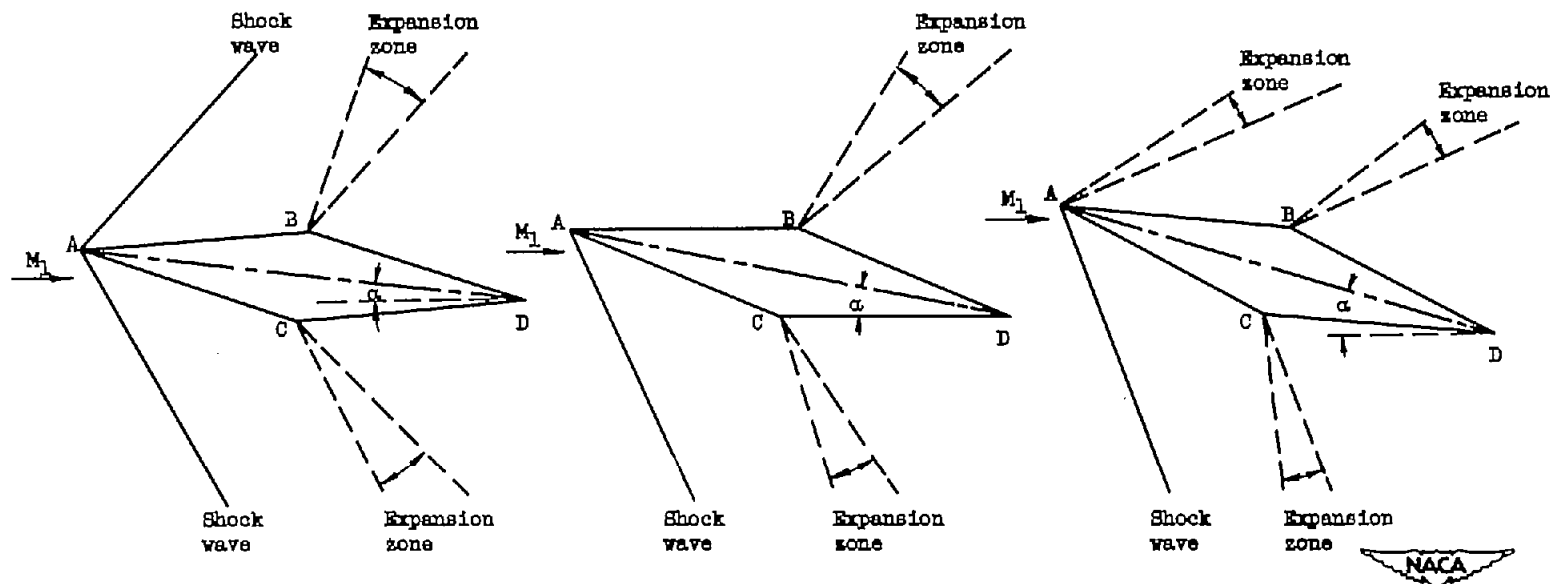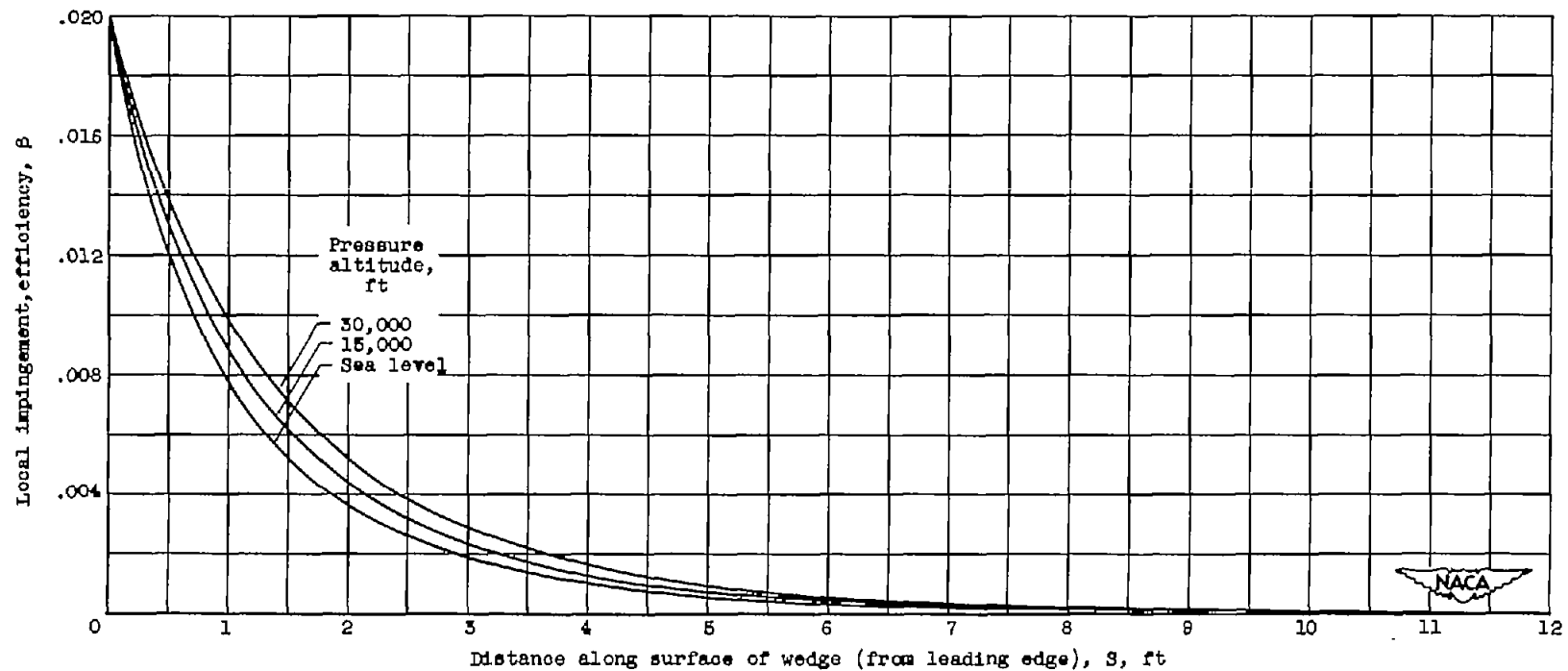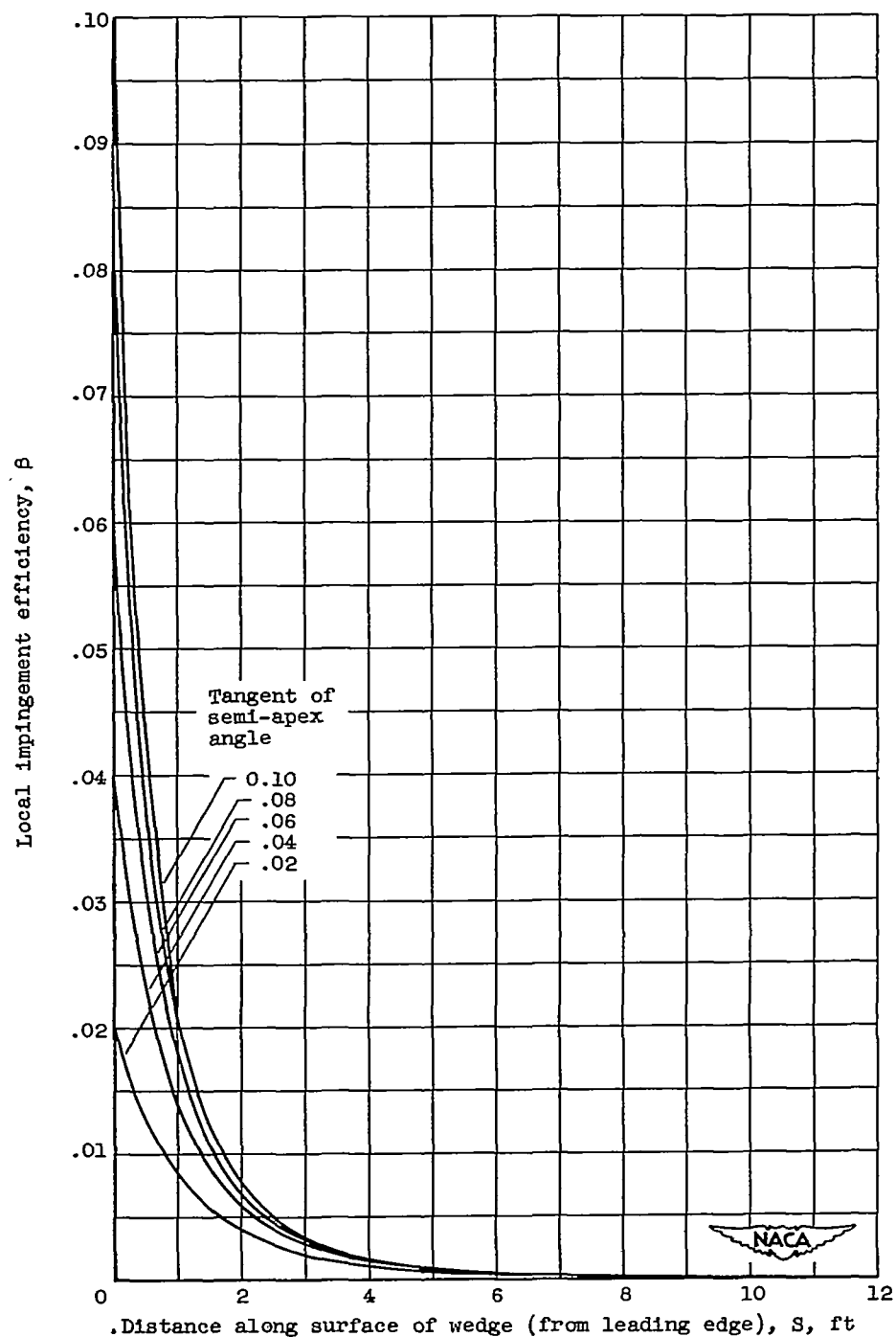
(a) Angle of attack, $\alpha < \tan^{-1}(T/c)$.   (b) Angle of attack, $\alpha = \tan^{-1}(T/c)$.   (c) Angle of attack, $\alpha > \tan^{-1}(T/c)$.

Figure 5. - Schematic diagram of diamond airfoil in supersonic flow with attached shock waves and at angle of attack.

(a) Effect of pressure altitude. Droplet diameter, 20 microns; free-stream Mach number, 1.4; tangent of semi-apex angle, 0.02.
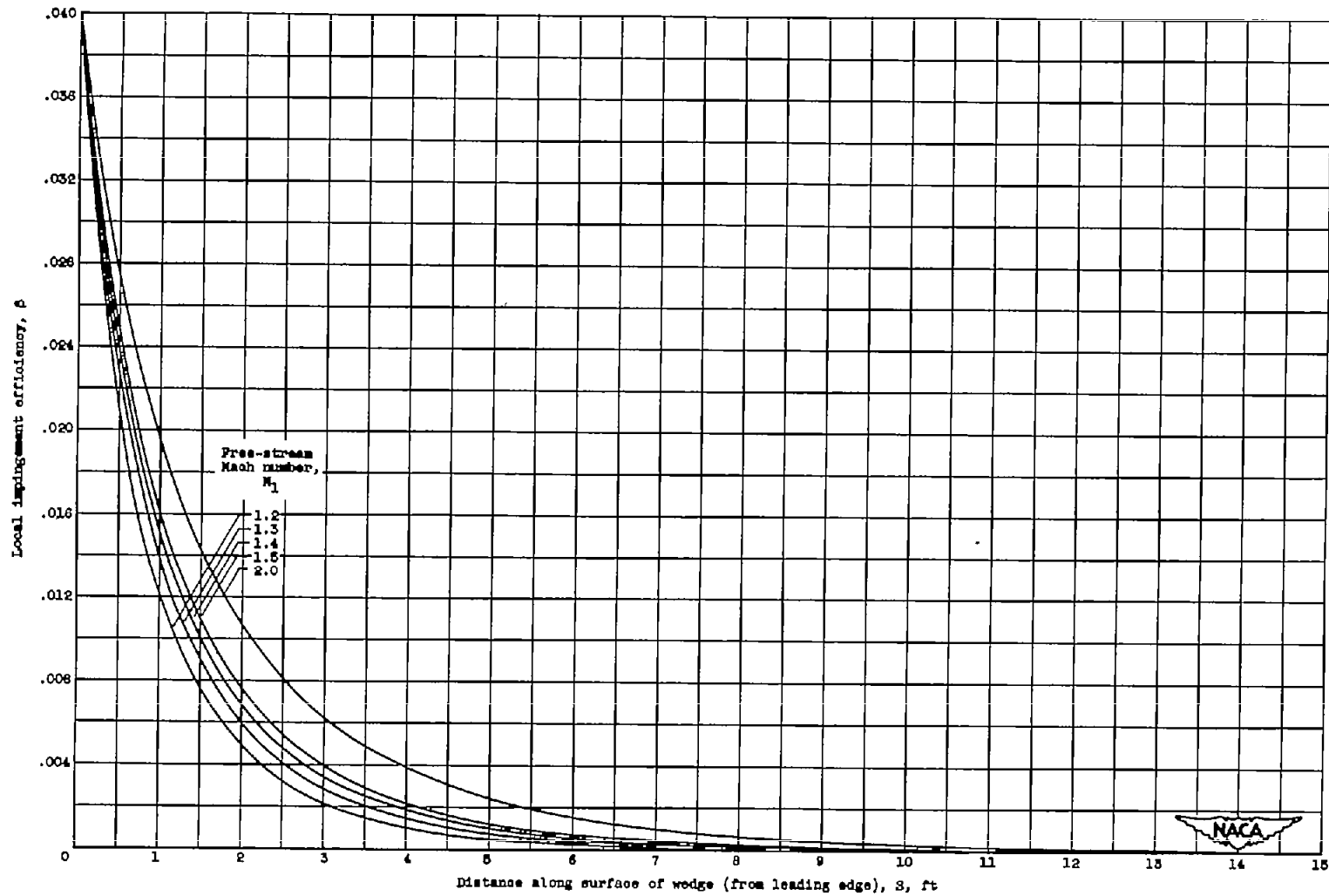
Figure 4. - Local impingement efficiency on wedge as function of distance along surface of wedge. Free-stream static temperature, 440° R.

(b) Effect of wedge semi-apex angle. Droplet diameter,
    20 microns; free-stream Mach number, 1.3; pressure
    altitude, 15,000 feet.

Figure 4. - Continued. Local impingement efficiency on wedge
    as function of distance along surface of wedge. Free-stream
    static temperature, 440° R.
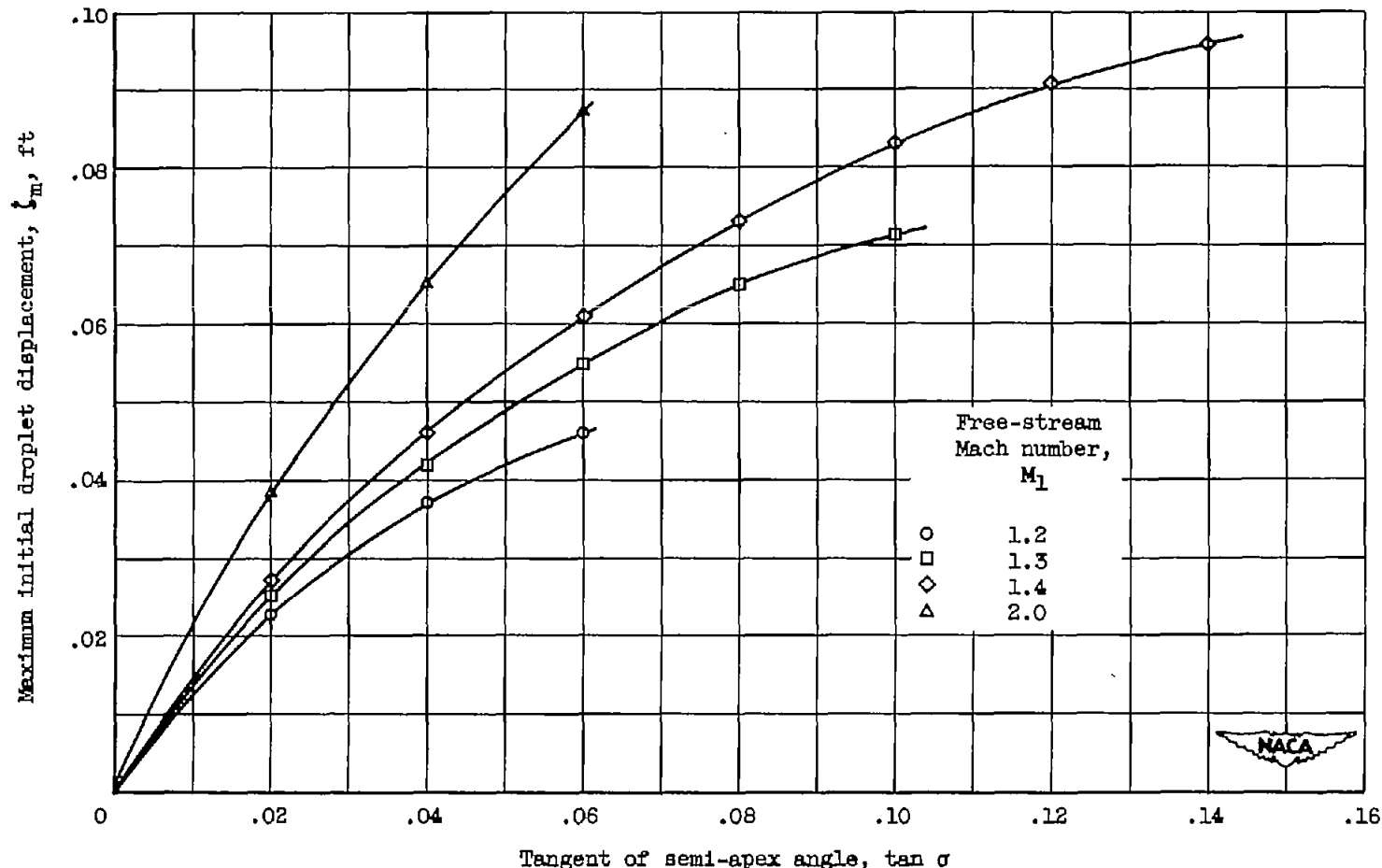
(c) Effect of free-stream Mach number. Droplet diameter, 20 microns; tangent of semi-apex angle, 0.04; pressure altitude, 15,000 feet.

Figure 4. - Continued. Local impingement efficiency on wedge as function of distance along surface of wedge. Free-stream static temperature, 440° R.
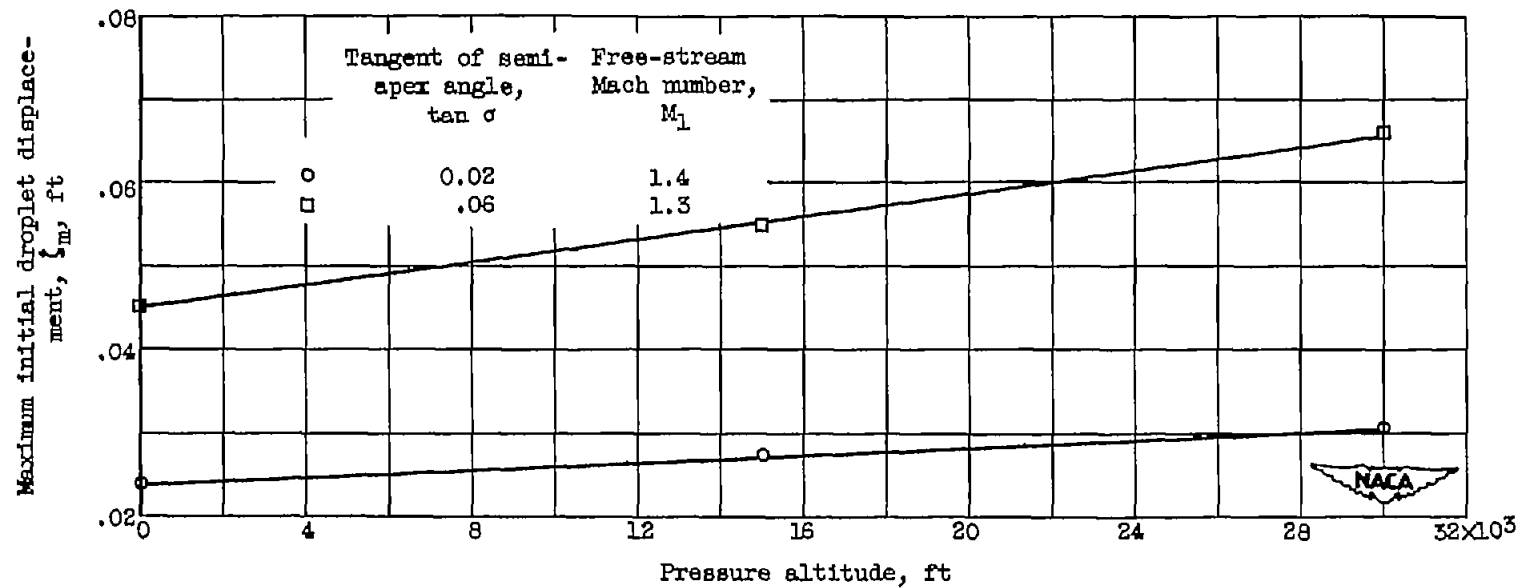
(d) Effect of droplet size. Free-stream Mach number, 1.3; tangent of semi-apex angle, 0.06; pressure altitude, 15,000 feet.

Figure 4. - Concluded. Local impingement efficiency on wedge as function of distance along surface of wedge. Free-stream static temperature, 440° R.

(a) Effect of tangent of semi-apex angle. Pressure altitude, 15,000 feet; droplet diameter, 20 microns.

Figure 5. - Total impingement rate W_m for wedge of infinite extent. Free-stream static temperature, 440° R. $W_m = 0.329\zeta_m V_1 w$.
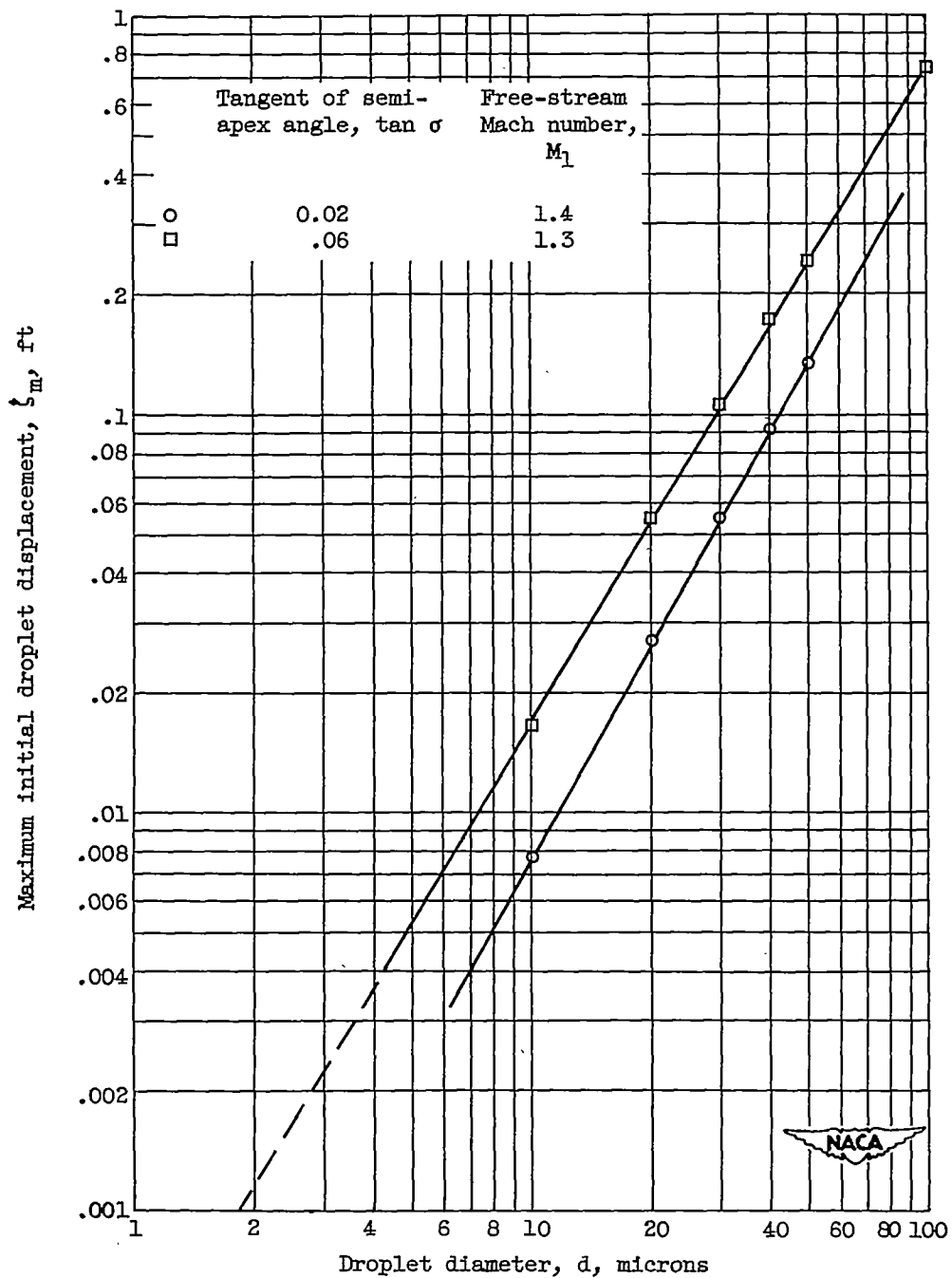
(b) Effect of pressure altitude. Droplet diameter, 20 microns.

Figure 5. - Continued. Total impingement rate W_m for wedge of infinite extent. Free-stream static temperature, 440° R. $W_m = 0.329\zeta_m V_1 w$.

(c) Effect of droplet size. Pressure altitude, 15,000 feet.

Figure 5. - Concluded. Total impingement rate W_m for wedge of infinite extent. Free-stream static temperature, 440° R. $W_m = 0.329 \zeta_m V_1 w$.

Ratio of impingement velocity of droplet to free-stream velocity, $V_{d,im}/V_1$

Tangent of semi-apex angle, tan σ	Free-stream Mach number, M_1	Pressure altitude, ft	Velocity ratio, V_2/V_1
0.02	2.0	15,000	0.988
.06	1.3	30,000	.919
.10	1.3	15,000	.844

Distance along surface of wedge (from leading edge), S, ft
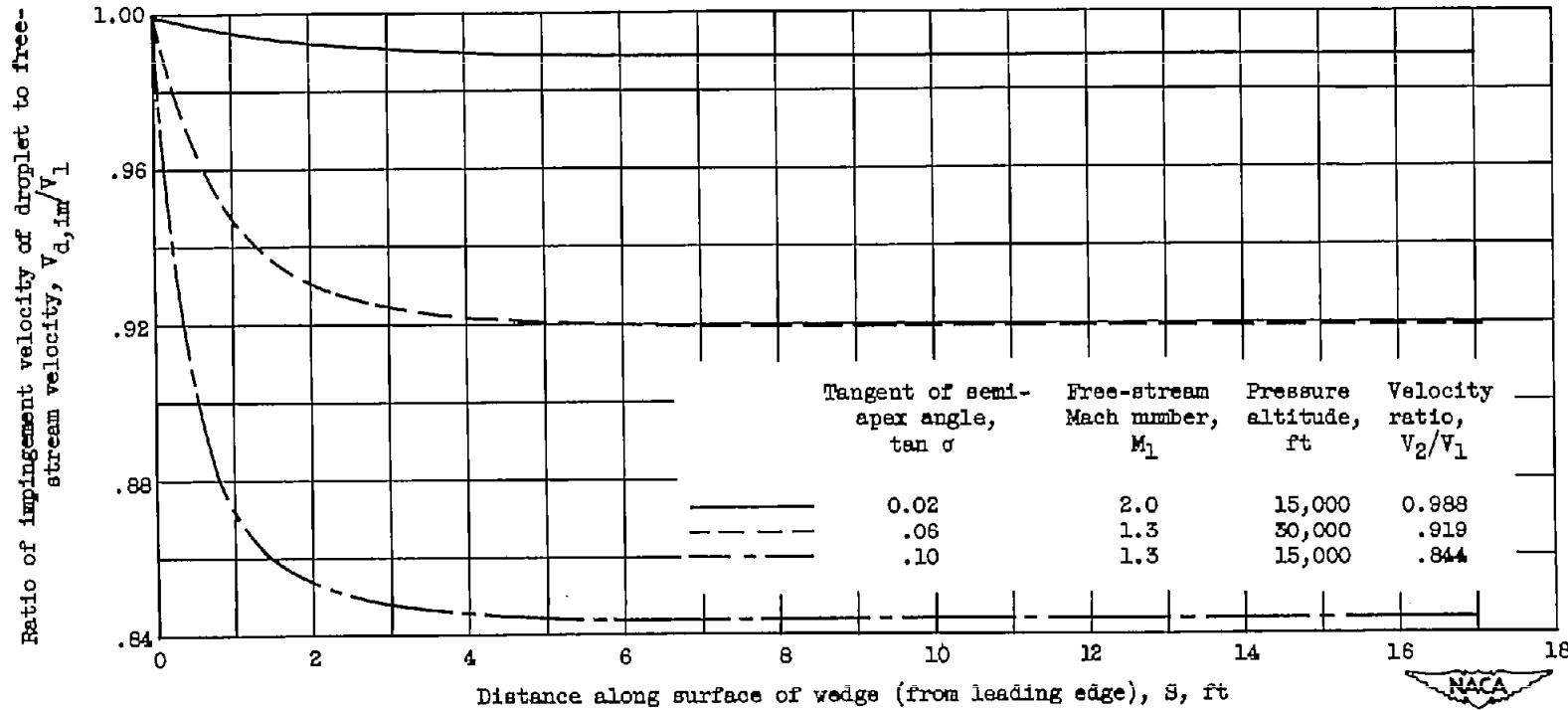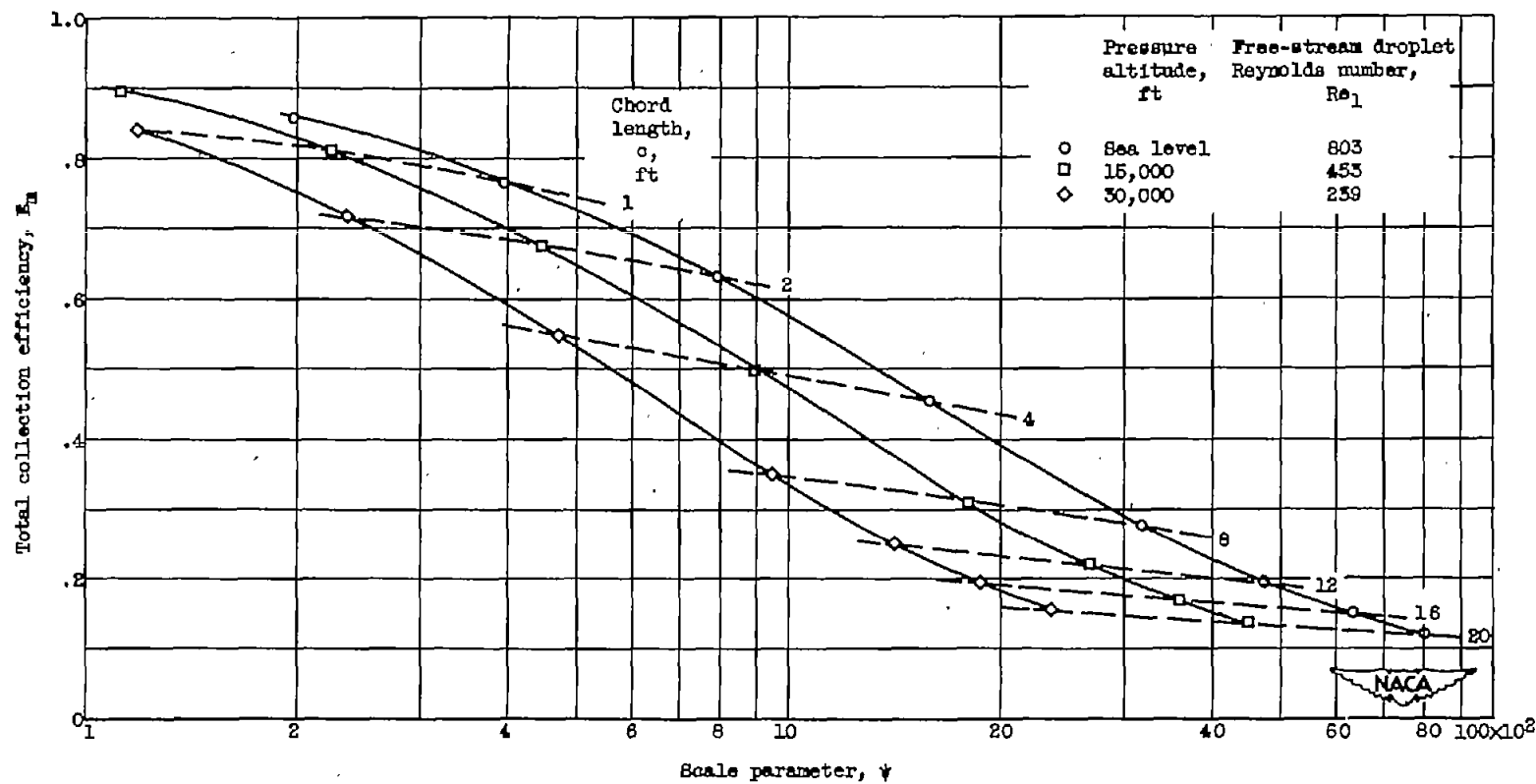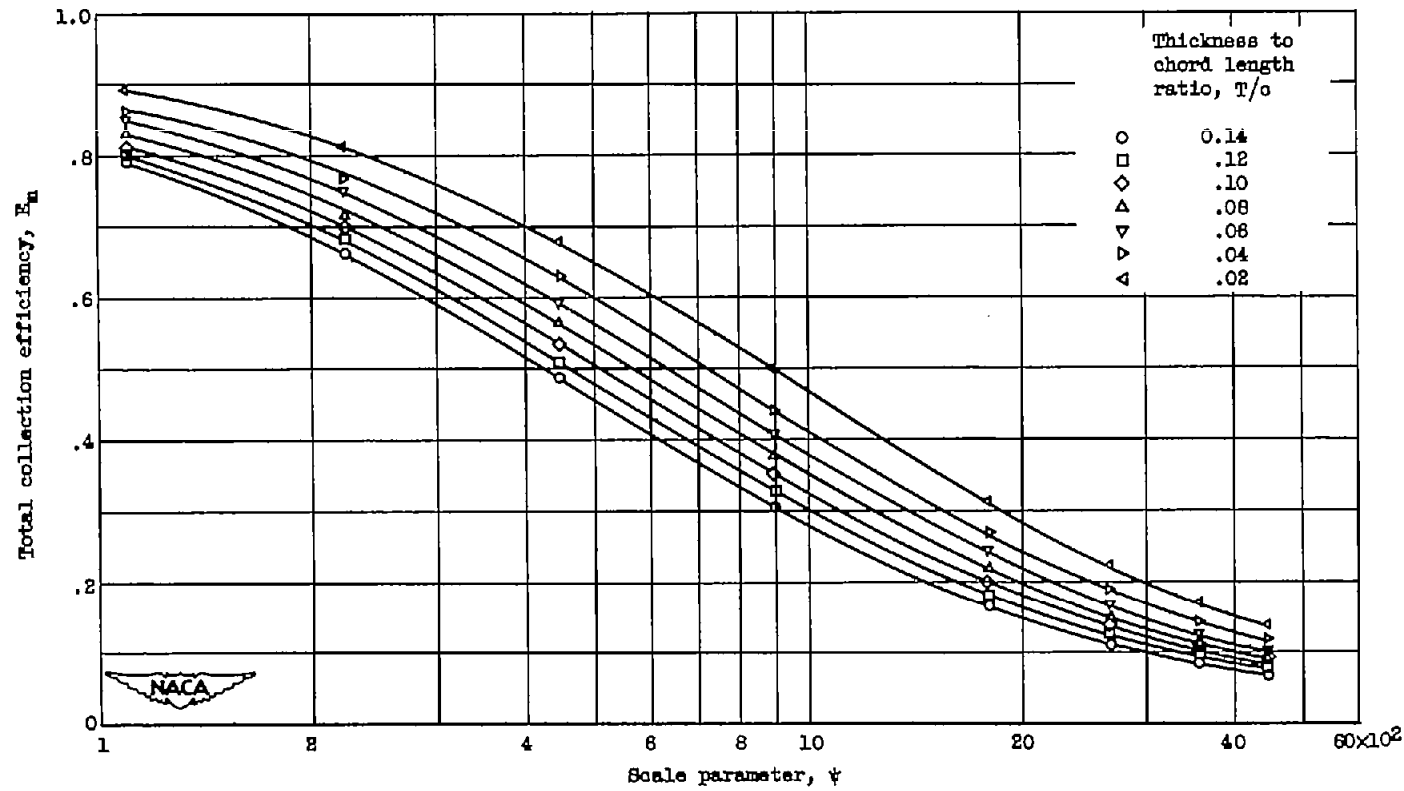
Figure 6. - Variation of ratio of impingement velocity of droplet to free-stream velocity with distance along surface of wedge. Free-stream static temperature, 440° R; droplet diameter, 20 microns.
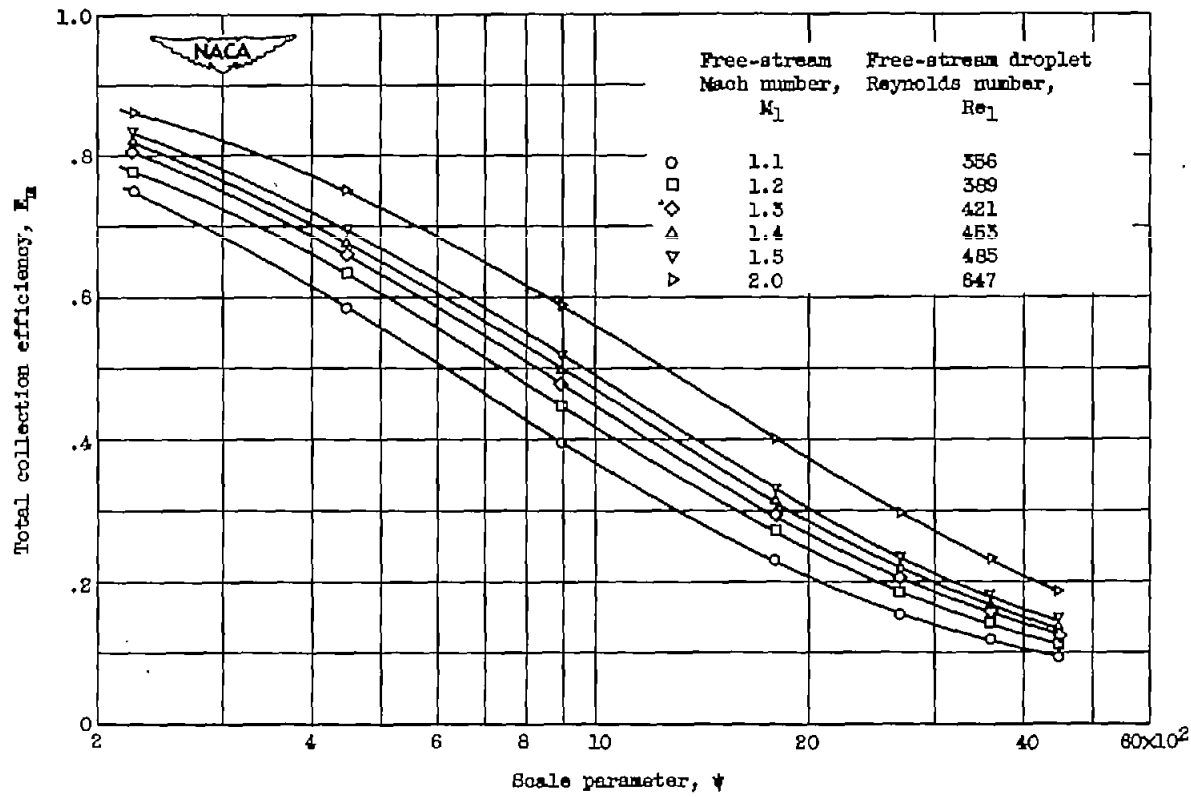
(a) Effect of pressure altitude and chord length. Diamond airfoil thickness, 2 percent; droplet diameter, 20 microns; free-stream Mach number, 1.4.

Figure 7. - Total collection efficiency of diamond airfoils as function of scale parameter. Free-stream static temperature, 440° R; angle of attack, 0°.
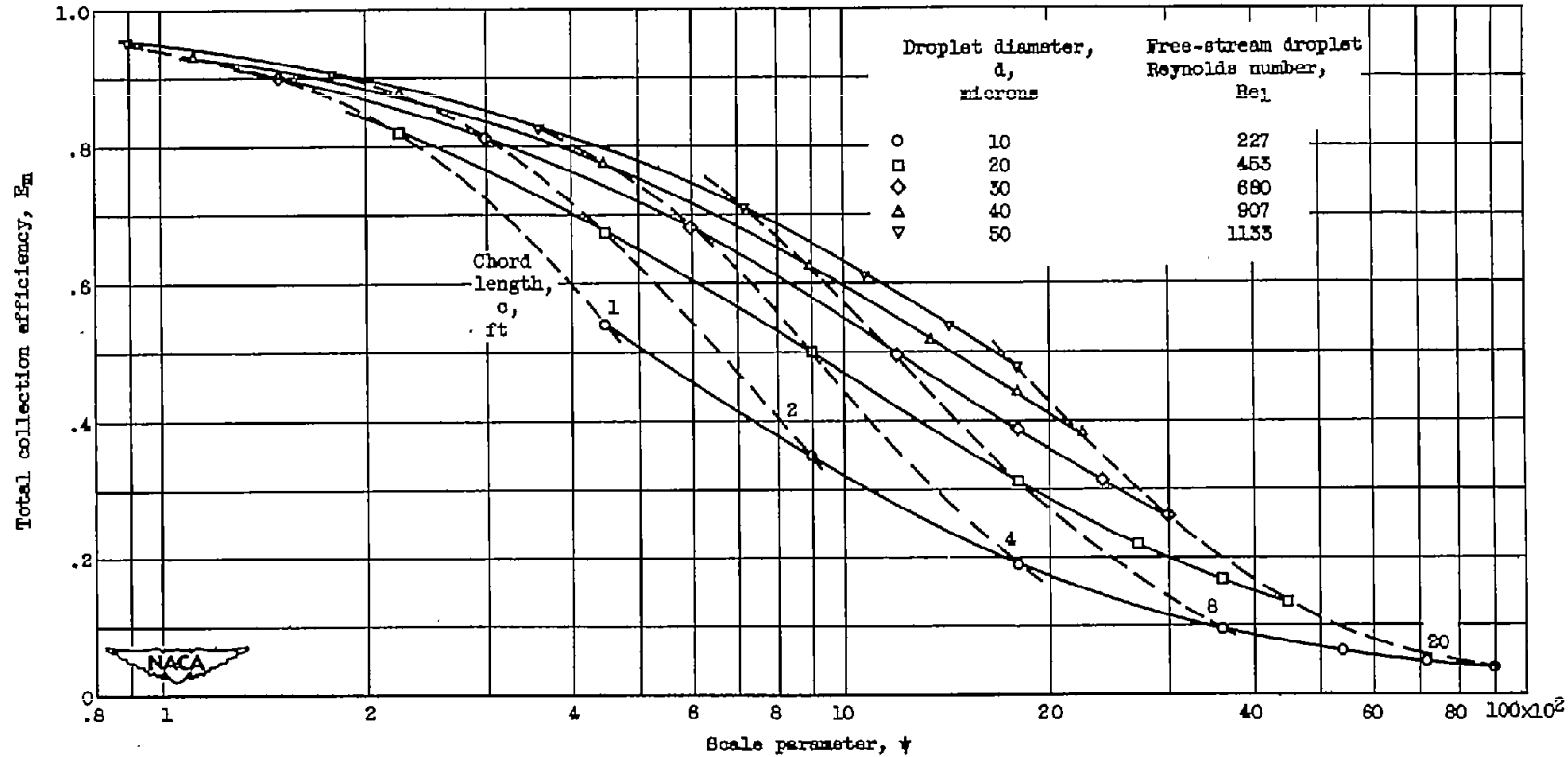
(b) Effect of thickness ratio of diamond airfoils. Droplet diameter, 20 microns; free-stream Mach number, 1.4; free-stream droplet Reynolds number, 453; pressure altitude, 15,000 feet.

Figure 7. - Continued. Total collection efficiency of diamond airfoils as function of scale parameter. Free-stream static temperature, 440° R; angle of attack, 0°.
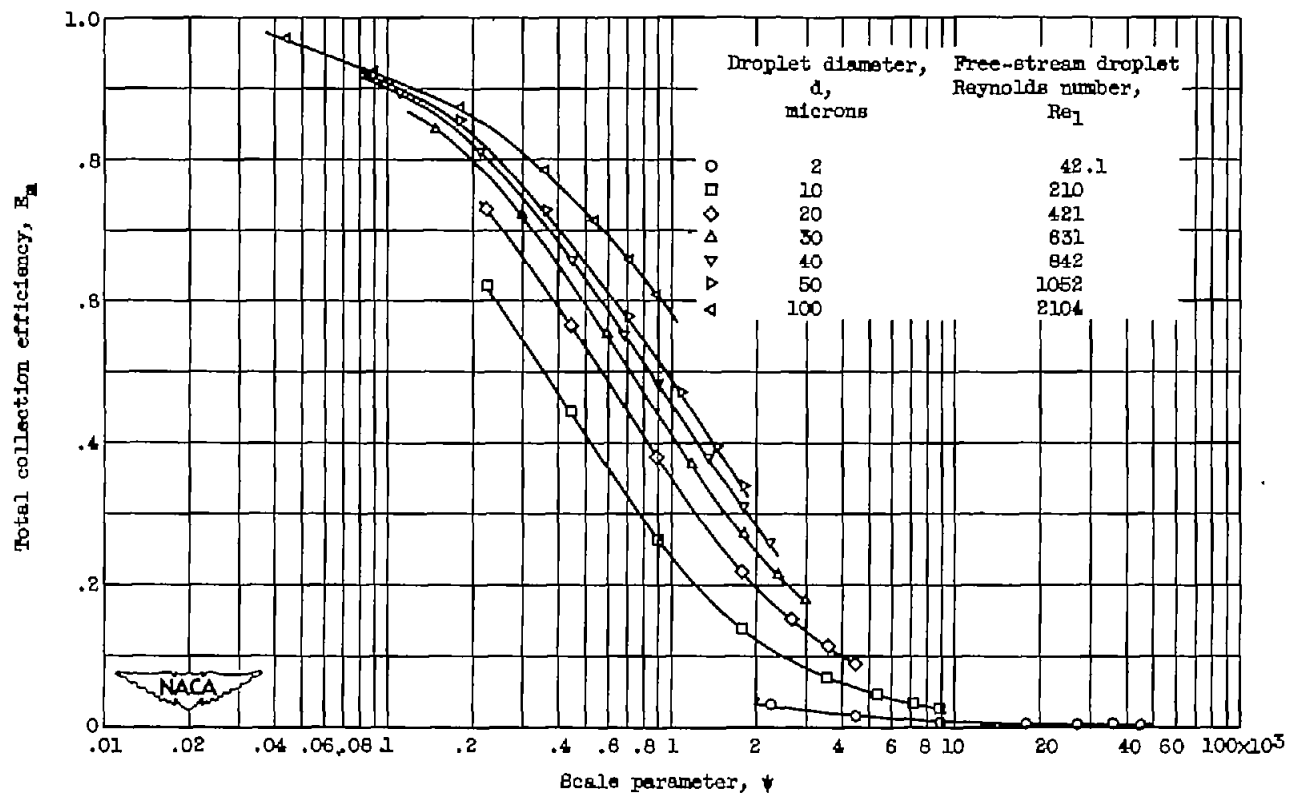
(c) Effect of free-stream Mach number. Diamond airfoil thickness, 2 percent; droplet diameter, 20 microns; pressure altitude, 15,000 feet.

Figure 7. - Continued. Total collection efficiency of diamond airfoils as function of scale parameter. Free-stream static temperature, 440° R; angle of attack, 0°.

(d) Effect of droplet size and chord length. Diamond airfoil thickness, 2 percent; free-stream Mach number, 1.4; pressure altitude, 15,000 feet.

Figure 7. - Continued. Total collection efficiency of diamond airfoils as function of scale parameter. Free-stream static temperature, 440° R; angle of attack, 0°.

(e) Effect of droplet size. Diamond airfoil thickness, 6 percent; free-stream Mach number, 1.3; pressure altitude, 15,000 feet.

Figure 7. - Concluded. Total collection efficiency of diamond airfoils as function of scale parameter. Free-stream static temperature, 440° R; angle of attack, 0°.
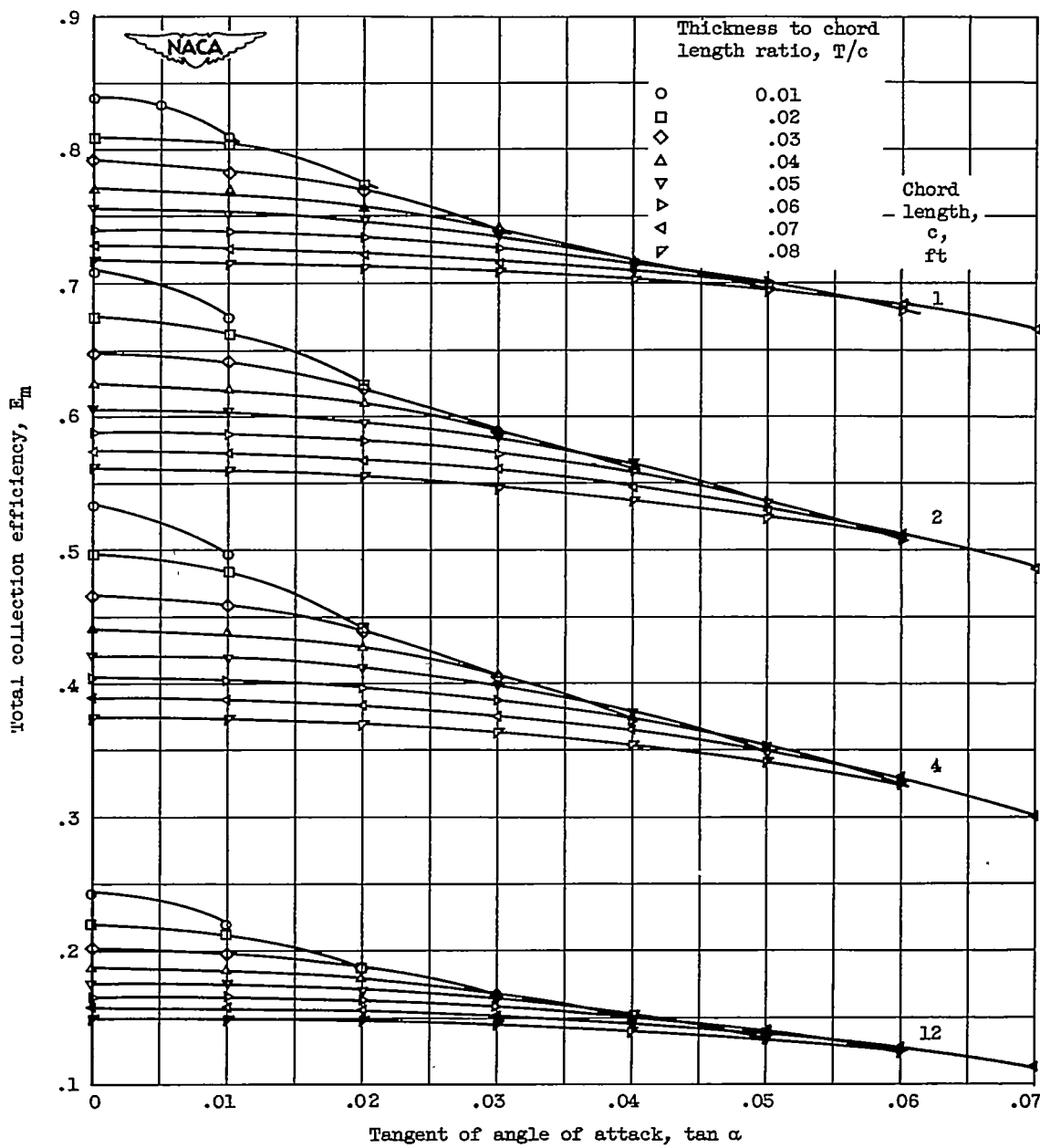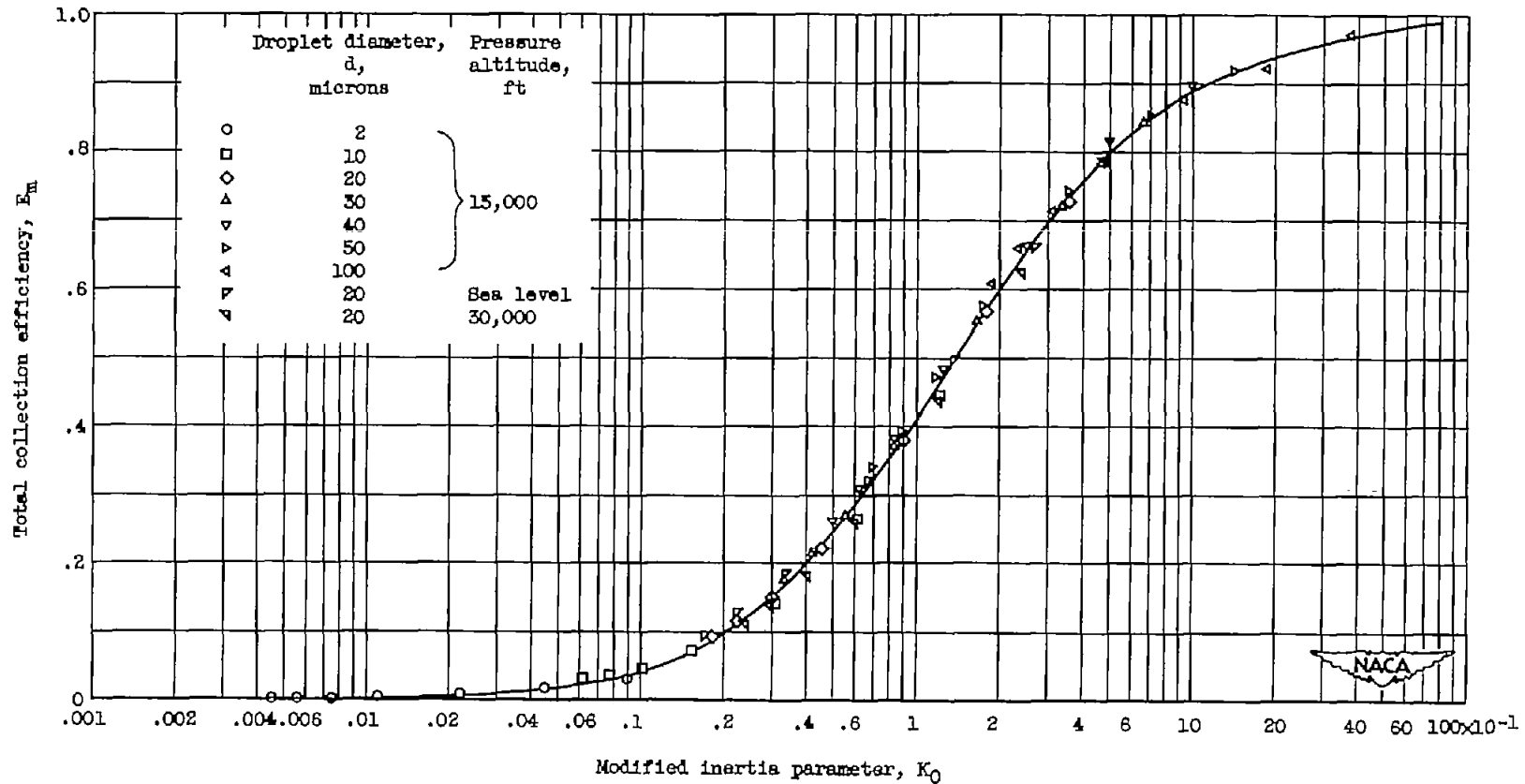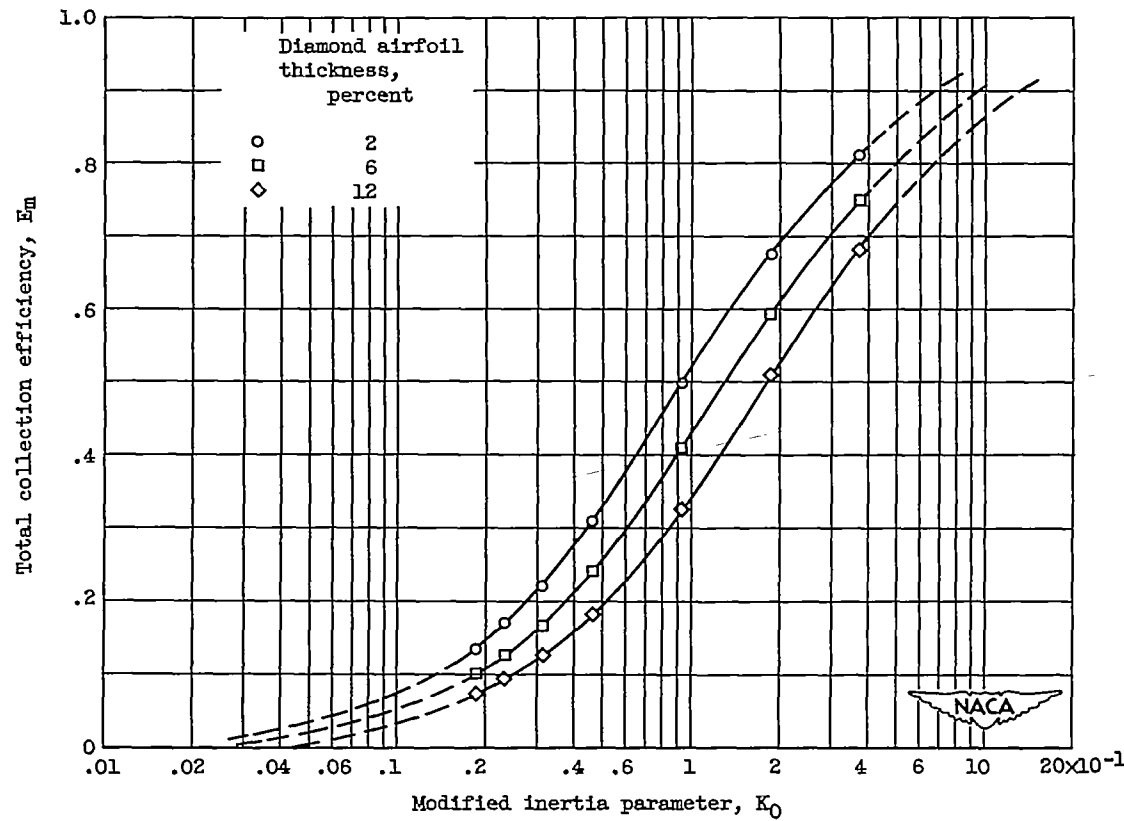
Figure 8. - Variation of total collection efficiency with angle of attack. Free-stream static temperature, 440° R; droplet diameter, 20 microns; free-stream Mach number, 1.4; pressure altitude, 15,000 feet.
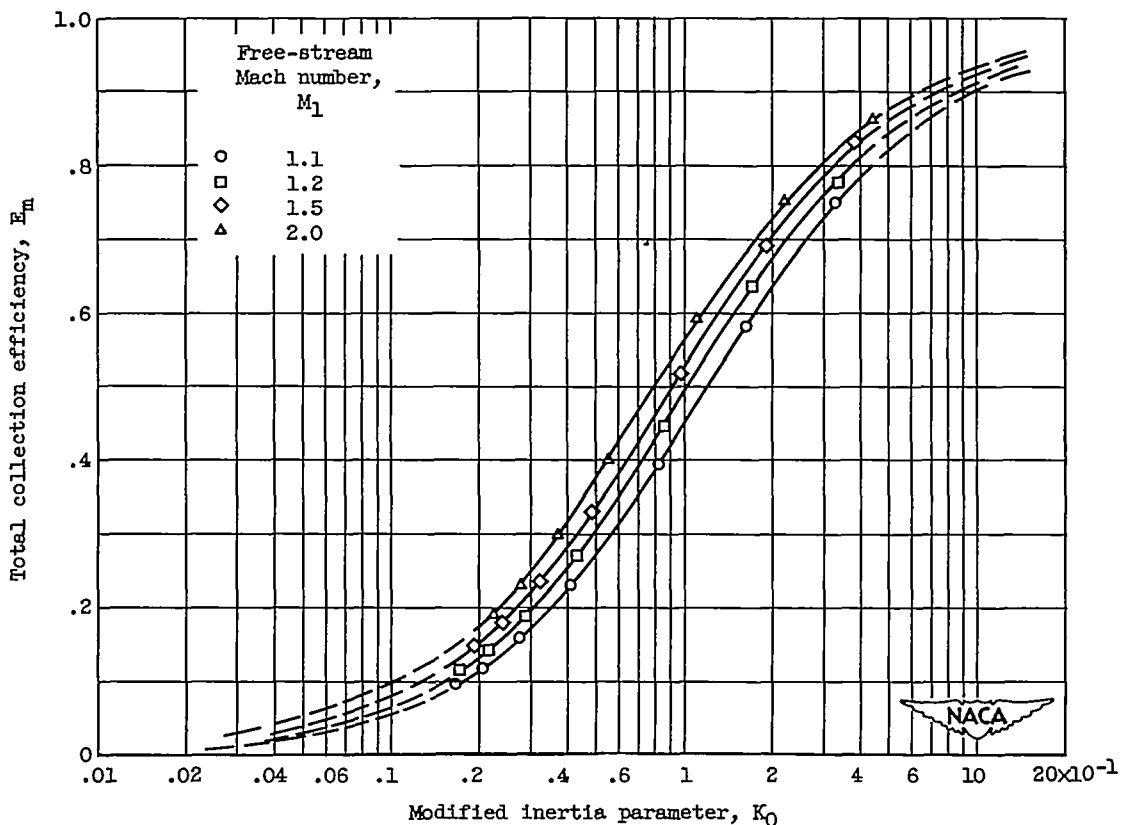
(a) Correlation of pressure altitude and droplet size. Diamond airfoil thickness, 6 percent; free-stream Mach number, 1.3.

Figure 9. - Total collection efficiency of diamond airfoils as function of modified inertia parameter. Free-stream static temperature, 440° R; angle of attack, 0°.

(b) Effect of diamond airfoil thickness ratio. Free-stream Mach number, 1.4;
   droplet diameter, 20 microns; pressure altitude, 15,000 feet.

Figure 9. - Continued. Total collection efficiency of diamond airfoils as func-
   tion of modified inertia parameter. Free-stream static temperature, 440° R;
   angle of attack, 0°.

(c) Effect of free-stream Mach number. Diamond airfoil thickness, 2 percent; droplet diameter, 20 microns; pressure altitude, 15,000 feet.

Figure 9. - Concluded. Total collection efficiency of diamond airfoils as function of modified inertia parameter. Free-stream static temperature, 440° R; angle of attack, 0°.
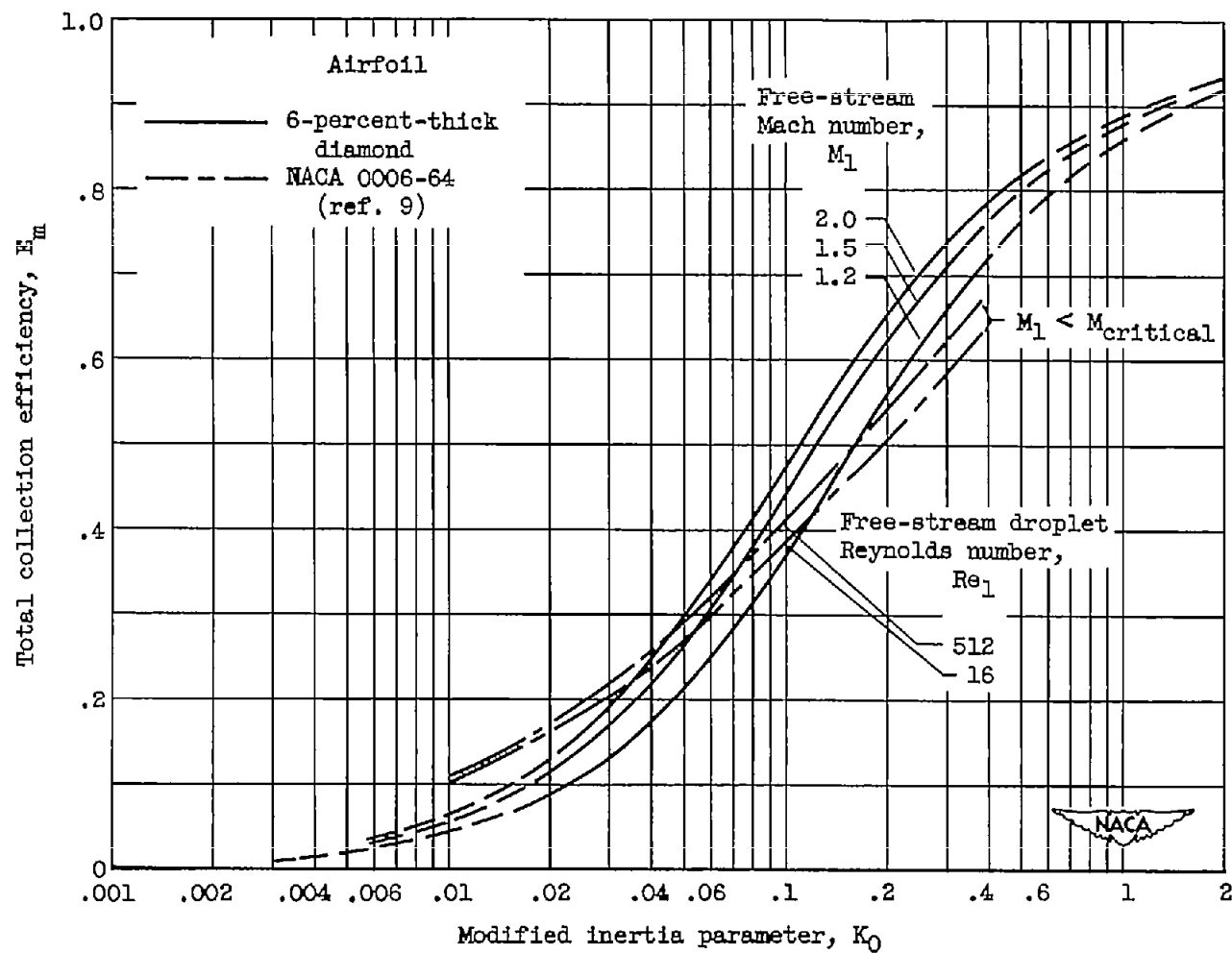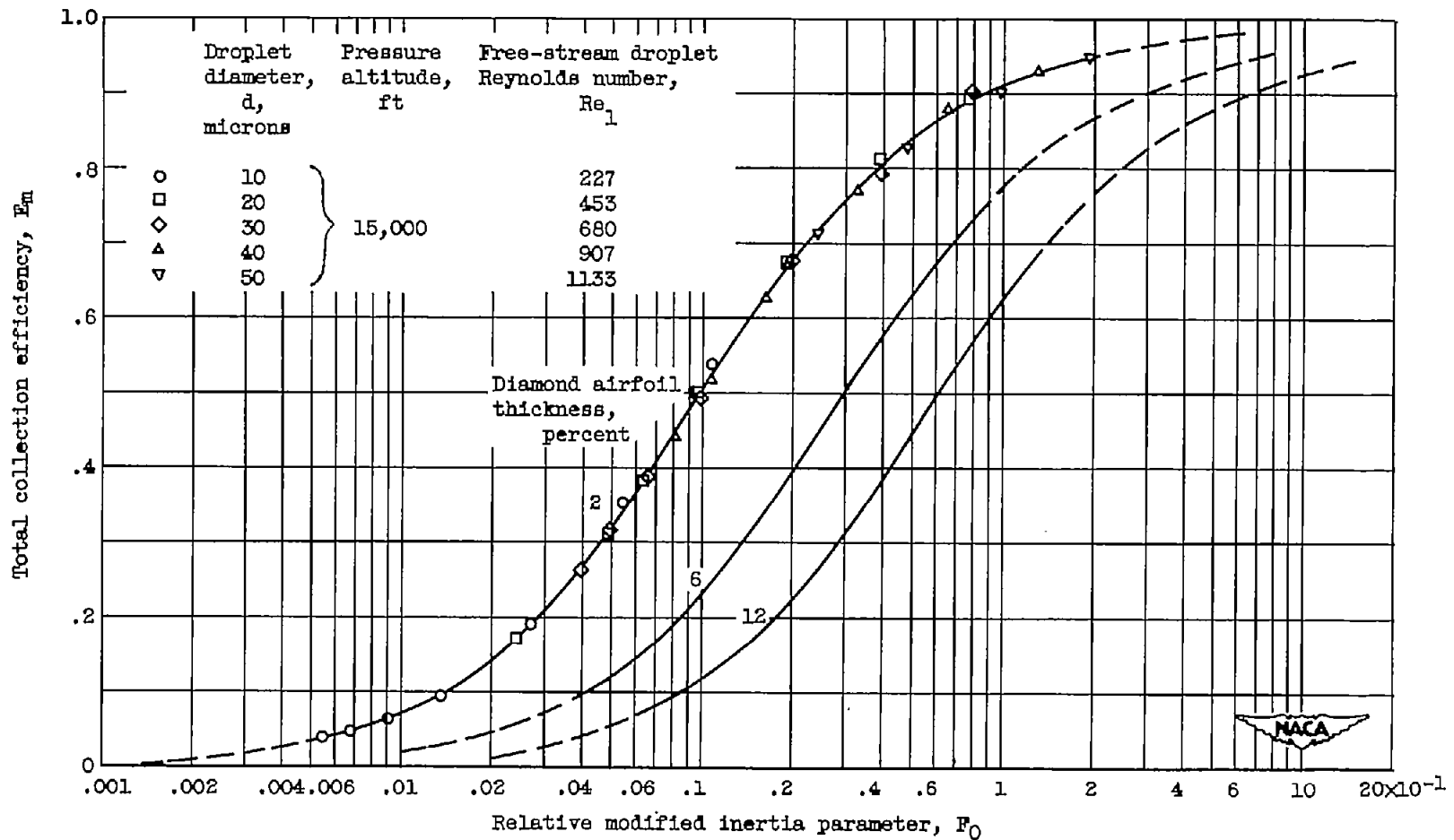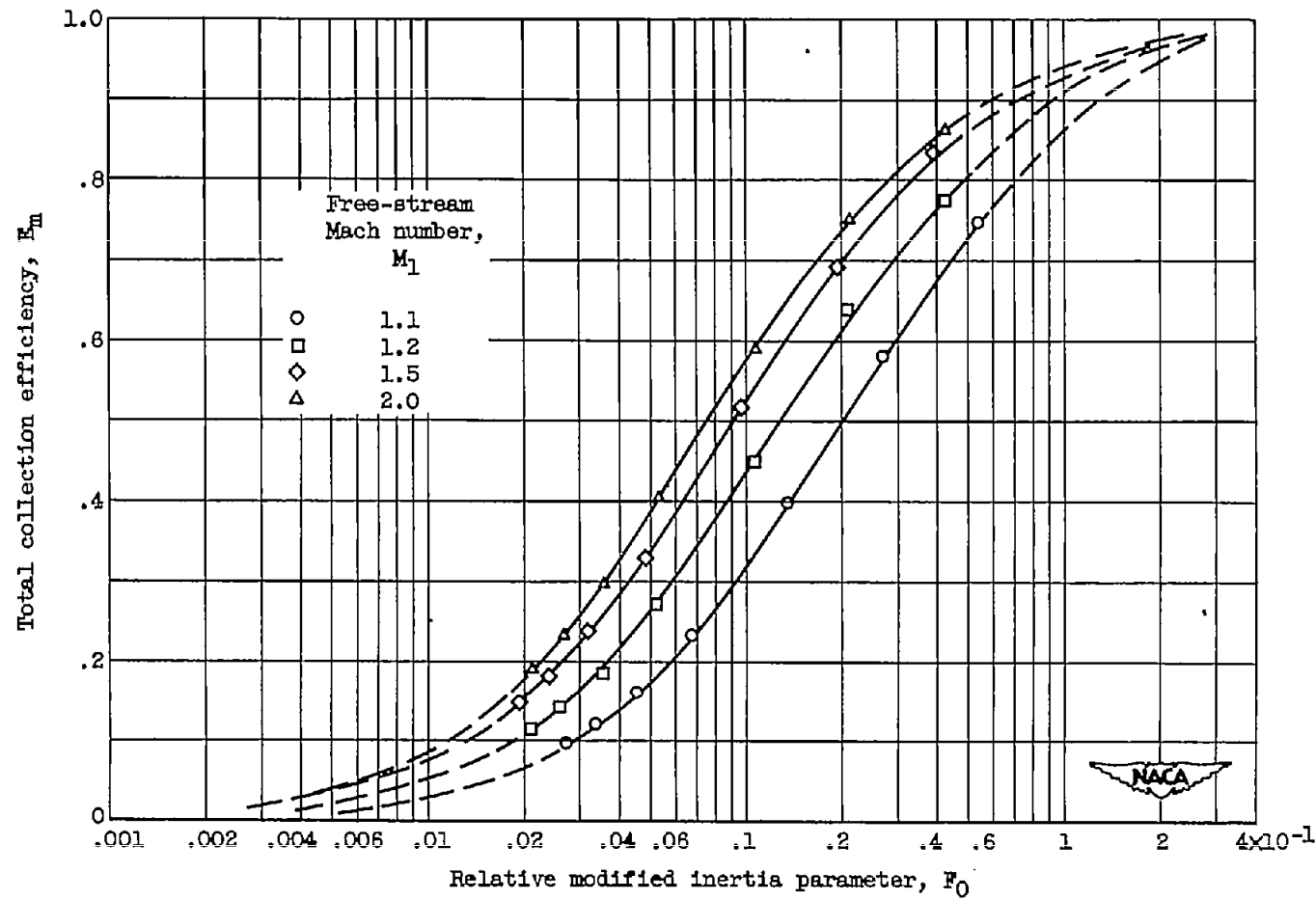
Figure 10. - Comparison of total collection efficiency as function of modified inertia parameter for diamond airfoil at supersonic speeds (attached shock wave) with that for NACA 0006-64 airfoil at free-stream Mach numbers less than critical. Airfoil thickness, 6 percent; angle of attack, 0°.

(a) Effect of diamond airfoil thickness ratio. Free-stream Mach number, 1.4.

Figure 11. - Total collection efficiency of diamond airfoils as function of relative modified inertia parameter. Free-stream static temperature, 440° R; angle of attack, 0°.

(b) Effect of free-stream Mach number. Diamond airfoil thickness, 2 percent; droplet diameter, 20 microns; pressure altitude, 15,000 feet.

Figure 11. - Concluded. Total collection efficiency of diamond airfoils as function of relative modified inertia parameter. Free-stream static temperature, 440° R; angle of attack, 0°.